Massively parallelized molecular force manipulation with on demand thermal and optical control

Hanquan Su[1,4] Joshua M. Brockman[2,4] Yuxin Duan[1,4] Navoneel Sen[3] Hemani Chhabra[3] Alisina Bazrafshan[1] Aaron T. Blanchard[2] Travis Meyer[2] Brooke Andrews[1] Jonathan P.K. Doye[3] Yonggang Ke[1,2] R. Brian Dyer[1] Khalid Salaita[1,2,*]

[1]Department of Chemistry, Emory University, Atlanta, Georgia, 30322, United States. [2]Wallace H. Coulter Department of Biomedical Engineering, Georgia Institute of Technology and Emory University, Atlanta, Georgia, 30322, United States. [3]Physical and Theoretical Chemistry Laboratory, Department of Chemistry, University of Oxford, South Parks Road, Oxford OX1 3QZ, United Kingdom. [4]These authors contributed equally to this work.

*Correspondence should be addressed to K.S. (k.salaita@emory.edu)

This PDF file includes:

Materials and Methods
Note S1-S3
Figure S1-S13
Table S1-S6

Materials and Methods

Reagents

All reagents were purchased from Sigma-Aldrich (St. Louis, MO) and were used as received, unless otherwise stated. N,N'-methylenebisacrylamide was purchased from Alfa Aesar (Haverhill, MA). Cy3B-NHS ester was purchased from GE healthcare Bio-Science (Pittsburgh, PA). Tris-hydroxypropyltriazolylmethylamine (THPTA) was purchased from Click Chemistry Tools (Scottsdale, AZ 85260). DMSO (99.5%) and sodium bicarbonate (99.0%) were acquired from EMD chemicals (Philadelphia, PA). P4-gel size exclusion beads were acquired from Biorad (Hercules, CA). Gold nanorods (AuNRs) were synthesized in-house and characterized by TEM. Based on TEM analysis, the mean diameter of AuNRs was 25 × 100 nm. Milli-Q water was obtained from a Nanopure system with 18.2 M^{-1}-cm resistivity. All oligonucleotides were purchased from Integrated DNA Technologies (Coralville, IA) and were purified either by reverse-phase HPLC or standard desalting.

Synthesis of origami-polymer force clamp

First, cetyltrimethylammonium bromide (CTAB) stabilized AuNRs (size = 25 x 100 nm) were synthesized according to the protocol reported by Murray and colleagues[1]. After synthesis, the reaction mixture (~ 200 ml) was centrifuged at 5000 rpm for 60 min and the supernatant was discarded. The AuNRs were resuspended in 90 ml of DI water (concentration = ~1 nM). CTAB was exchanged with N, N'-bis(acryloyl)cystamine (20 mg dissolved in 10 ml ethanol) by vigorous stirring (700 rpm) for 12 h. Next, 15 ml Milli-Q water was heated to 70 ℃ with N_2 purging in a three-neck flask. Next, 0.1 g of N-isopropylmethacrylamide and 0.01 g of the crosslinking agent N,N'-methylenebisacrylamide were dissolved in 15 ml Milli-Q water with vigorous stirring and continuously purged with N_2 flow. Next, 7 ml of the AuNR solution (described above, ~ 1 nM) were centrifuged at 6500 rpm for 10 min, the supernatant was removed and AuNRs were dispersed in 1 ml Milli-Q water and added to the reaction flask. Within 2 min, polymerization was initiated with the addition of 80 μl of 0.1 M of the free radical initiator, 2,2'azobis(2-methylpropionamidine) dihydrochloride (AAPH). The reaction proceeded for 2 h and the alkyne functional group was introduced via dropwise injection of 0.01 ml of propargyl methacrylate monomer (80 μmol). After 1 h, the reaction was stopped, and the turbid pNIPMAm particle solution was cooled to room-temperature. The product was centrifuged and dispersed in Milli-Q water. This was repeated at least three times to ensure sufficient removal of unreacted monomer. The core-shell structure and mono-dispersity of pNIPMAm particles were verified by TEM and dynamic light scattering (DLS) analysis, respectively. The particle concentration was calculated using Beer Lambert law. As reported by Christopher J. Orendorff and Catherine J. Murphy[2], the extinction coefficient of gold nanorods (42 x 12.3 nm, λ = 785nm) $\varepsilon_{785\ nm} = 4.6 \times 10^9\ M^{-1}cm^{-1}$. Because the size of AuNR in this work is ~ twice that of the reported values in all dimensions (L x W x H), we approximated the extinction coefficient of 25 x 100 nm AuNR to be $\varepsilon_{785\ nm} = 2^3 \times 4.6 \times 10^9\ M^{-1}cm^{-1} = 3.7 \times 10^{10}\ M^{-1}cm^{-1}$.

The pNIPMAm particles were then decorated with single-stranded DNA (ssDNA) to facilitate the particle-DNA origami assembly. Briefly, 25μl of pNIPMAm particles (~1.25nM) and 25μl of ssDNA (*b**, 100μM) was mixed in a 1.5ml Eppendorf tube. Then, in a separate tube, 5μl of $CuSO_4$ (20mM) was added to 10μl of THPTA (50mM) solution to form a blue-colored Cu-THPTA complex (ligand to copper ratio is 5:1). Finally, 5μl of Cu-THPTA complex was reduced by adding 5μl of 100mM freshly prepared sodium ascorbate solution (blue color to clear) and the mixture was added to the first tube containing pNIPMAm particle and ssDNA. Note that the Cu-THPTA needs to be reduced by sodium ascorbate before mixing with particle and ssDNA. The reaction was left at RT for 1 hour and washed 5 times by centrifugation at 5000 rpm for 6 mins.

The origami template was assembled from single-stranded scaffold p7560, which was prepared from M13 phage using a previously reported method [3-4]. A 16-helix bundle (16HB) rod was designed in caDNAno, based on a 4 x 4 square lattice cross-section. To synthesize 16HB structure and incorporate DNA hairpin to 16HB, a 10-fold excess of staple strands (100 nM) and 15-fold excess of DNA hairpins (150nM) were mixed with p7560 scaffold strand (10 nM) in folding buffer (5 mM Tris, 1 mM EDTA, 10 mM $MgCl_2$ with a total volume of 50 µL. The mixture was denatured at 85℃ for 10 min, followed by a slow anneal from 60 ºC to 25 ºC over 18 hrs (-2ºC/hr). 16HB were purified from excess staples using agarose gel electrophoresis (0.67%) in 0.5X TBE+Mg buffer (45 mM Tris, 45 mM Boric acid, 1 mM EDTA, 10 mM $MgCl_2$). PEG precipitation was used to purify 16HB from excess staples in large scale synthesis (30nM). Briefly, the 16HB solution was mixed with precipitation buffer (15% PEG8000, 1x TE, 505mM NaCl, 10mM $MgCl_2$) at a 1:1 ratio. Samples were centrifuged at ~16,000g for 25 minutes at 4 ºC (there should be a pellet after centrifugation). Then the supernatant was removed, and DNA origami was resuspended with folding buffer. 16HB structures were characterized by agarose gel electrophoresis (1.5%) and negative stain TEM imaging (1% uranyl formate).

Assembly of origami-polymer force clamp

15 µl of pNIPMAm particles (~0.3 nM) were mixed with 50 µl of 16HB origami beams (~30 nM). The mixture was incubated overnight at room temperature. The solution was then centrifuged at least 5 times at 5000 rpm for 6 mins. Finally, the sample was re-dispersed in ~ 40 µl buffer B (5 mM Tris-HCl, 10 mM $MgCl_2$ and 1 mM EDTA at pH = 8). This translates to ~10^9 OPFCs (0.3 nM * 15 µl * N_A), ~10^{11} origami beams (~200 origami structures on each particle), and ~10^{12} target molecules.

Transmission electron microscopy (TEM)

TEM measurements were acquired on a Hitachi H-7500 transmission electron microscope at an accelerating voltage of 80 kV in the Robert P. Apkarian Integrated Electron Microscopy Core at Emory University. A 5 µl sample (AuNRs or OPFCs) was deposited onto a 200-mesh carbon coated copper grid (Electron Microscopy Sciences). After 60 sec of incubation, excess liquid was wicked away. This incubation step was repeated three times. OPFCs sample preparation, negative staining was used after the sample incubation step described above. The specimens were stained by adding 5 µl of 1% uranyl formate solution onto the TEM grid. After 60 sec incubation, the excess liquid was wicked away. The sample grids were subsequently dried and stored in a desiccator.

DNA labeling

A mixture of oligonucleotide (0.01 ml, 10 nmol) and excess Cy3B-NHS ester (0.05 mg dissolved in 0.01 ml DMSO) in 0.1 M sodium bicarbonate solution (0.08 ml) was reacted at room-temperature for 12 h. The product was subjected to P4-gel filtration to desalt and to remove salts and unreacted dye. Reverse phase HPLC (solvent A: 0.1 M TEAA, solvent B: 100% MeCN; initial condition was 10% B with a gradient of 1 %/min, flow rate: 1 ml/min) was applied to further purify the product. Reaction products were purified using a L10NM8 column (diameter: 4.6 mm; length: 250 mm) in a reverse phase binary pump HPLC that was coupled to a diode array detector (Agilent 1100).

Equilibrium fluorescence measurements

Fluorescence spectra of Cy3B labeled DNA hairpin were obtained on the Dual-Fl Fluorometer (Horiba Scientific, Edison, New Jersey) with a 520 nm excitation. The samples were prepared at a concentration of 150 nM. Temperature dependent spectra were obtained from 20 ºC to 90 ºC in increments of 2.5 ºC using a peltier temperature controller. The solution temperature was held for 2 mins before collecting steady-state fluorescence spectra of the hairpins at each temperature. The Cy3B fluorescence emission peak was acquired at 575 nm. Integration time = 5 sec, detector accumulation = 3.

Time-resolved T-jump fluorescence spectroscopy

Temperature-jump fluorescence relaxation experiments were performed on a custom-built instrument as previously described (*25, 51*). Briefly, a Q-switched Ho:YAG laser (AQS-Ho-YAG, IPG Phototonics Corp., Oxford, MA) was used to generate a temperature jump of approximately 8-10°C. Temperature jumps are generated from the H_2O absorbance bands in the far IR. Fluorescence emission was probed using ~490 nm excitation generated by frequency-doubled Ti:Sapphire (980 nm) pumped by a Chameleon laser (Coherent, Santa Clara, CA). Sample emission fluorescence was collected at ~90° to the CaF_2 chamber and focused through a bandpass filter (514 nm-570 nm). The emission was measured using a Hamamatsu R7518 photomultiplier tube (Hamamatsu Photonics K. K., Hamamatsu, Japan). The signal was digitized and averaged (3000 shots) by a using a Wavesurfer 62Xs-B oscilloscope (Teledyne LeCroy, Chestnut Ridge, NY).

Data acquisition

Temperature jump experiments were performed on the origami-polymer force clamp or the DNA hairpin samples in buffer B (5 mM Tris-HCl, 10 mM $MgCl_2$ and 1 mM EDTA) at pH = 8. This buffer has been reported for preserving the intact structure of DNA origami (*52*). Rhodamine B solution (150 nM) was used as a reference to determine the temperature jump. The temperature dependency of Rhodamine B fluorescence was calibrated on the temperature-jump setup with a 490 nm excitation. The temperature was adjusted via a water bath and held for 5 mins. Then, Rhodamine B fluorescence signal was recorded (using 3000 shots) and measured using the same instrumental setup and filters as those used for the T-jump and Force-jump measurements.

Note S1. Geometric analysis of DNA origami design parameters.

We used geometric calculations and chemo-mechanical modeling to assess the subset of the rod length and thickness parameter space that can conceivably result in particle collapse-drive tension probe opening. Specifically, we tested for length-thickness pairs that satisfied four conditions.

1. Two closed tension probes (positioned 15 nm from each end of the rod) need to be able to simultaneously bind to the relaxed particle. To test for this condition, we used the Petrosyan approximation of the worm-like-chain model [5] to calculate the closed tension probe's force-extension curve. We used this force-extension curve to find that $F = 4.7\ pN$ (which is equal to the probe's $F_{1/2}$[6]) when the closed tension probe's end-to-end extension is 17.3 nm. If the origami rod and the particle are treated as rigid and non-intersecting, then the length at which tethers can only

connect to the particle with a force $\geq 4.7\ pN$ (L_{cutoff}) can be calculated by re-arranging the equation:

$$17.3\ nm = \sqrt{(250\ nm)^2 + \left(\frac{L_{max}}{2} - (15\ nm)\right)^2} - (250\ nm) \qquad (1)$$

where 250 nm is the particle's radius. This yielded $L_{max} = 219\ nm$. This condition is satisfied only when $L \leq L_{max}$. This result would change with the particle's diameter or the length of the closed tension probe.

2. Closed tension probes need to be opened by particle collapse. To test for this condition, we tested all length-thickness pairs where the above condition was satisfied. Then, we checked to make sure that particle collapse (which results in a decrease of particle radius from 250 nm to 125 nm) could transfer the tension probe from a closed state (tether extension < 17.3 nm) to an opened state (tether extension > 17.3 nm). We found that when $L \leq 65\ nm$, particle collapse never caused tension probes to transition from a closed state to an open state. The regions of the length-thickness parameter space that fail to meet this or the previous condition are shown in green below.
3. Particle collapse should not result in "buckling" of the DNA origami rod. To test for this condition, we measured the critical buckling force (F_c) using an equation presented by Liedl *et. al* [7]:

$$F_c = \pi^2 P k_B T / L^2 \qquad (2)$$

where P is the persistence length of the bundle and $k_B T = 4.114\ pN\ nm$ is the Boltzmann's constant at room temperature. Based on a previous model presented by Castro *et. al* [8], we estimate P as $P = (53\ nm)\left(N_{duplex}\right)^{1.94}$ where N_{duplex} is the number of duplexes in the bundle. The region of the length-thickness parameter space that fails to meet this condition (e.g. $F_c \leq 4.7\ pN$) is shown in red below.

The above analysis also does not take into account that what's important for the bending of the origami is not simply the force being applied by a single hairpin, but the effective net force due to all the hairpins and linkers.

4. The rod should have dimensions that are appropriate for self-assembly. To test for this condition, we checked if the number of nucleotides in the rod, which we estimated as $LN_{duplex}/(0.34\ nm)$, was lower than 7,560 nt (the length of the scaffold used in this work). The region of the length-thickness parameter space that fails to meet this condition (e.g. $F_c \leq 4.7\ pN$) is shown with grey stripes above

We found that our selected condition ($N_{duplex} = 16$ and $L = 130\ nm$), denoted with a black dot in the figure below, satisfied all four of this conditions.

For the subset of the parameter space in which all four conditions were satisfied, we also estimated the fraction of tension probes that would be opened by particle collapse. To do this, we used Boltzmann distribution calculations to estimate the distribution of particle attachment points and then used the calculated Boltzmann distribution to estimate the percentage of tension probes that transition from a closed state to an opened state following particle collapse. We found that the percentage increased from ~0% to ~100% from $L \approx 65\ nm$ to $L \approx 125\ nm$, as shown via color within the figure below. These calculations were performed by assuming that the particle acts as a rigid sphere that decreases in size during collapse and that the rod is rigid as well. In reality, both structures likely undergo relaxation in response to force transmitted through the tension probes that will reduce the force experienced by the tension probes (and, by extension, reduce the fraction of tension probes that are opened by collapse). The OxDNA calculations further elaborate on this point.

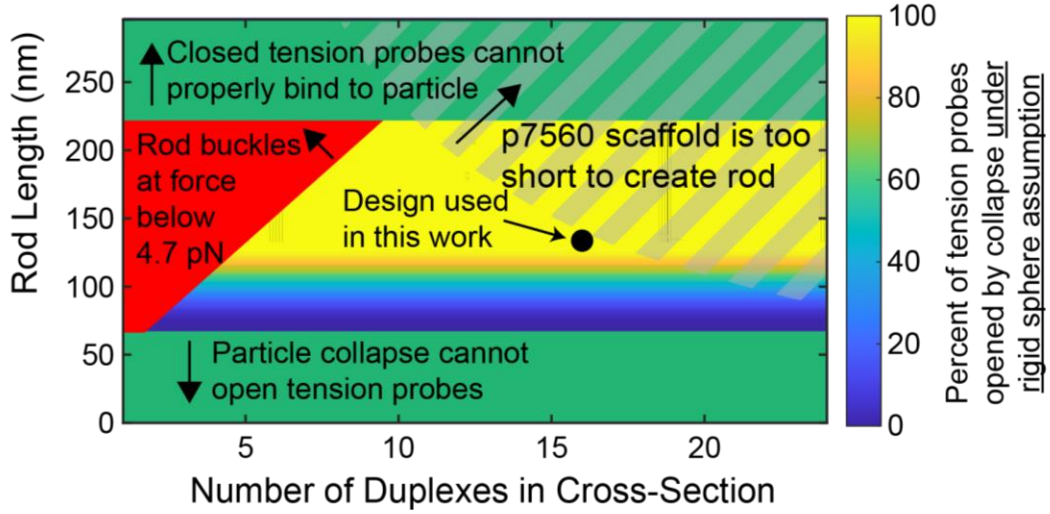

Note S2. Force calculation

Here, we considered the DNA hairpin as a classic two-state system, where a hairpin structure transformed between folded and unfolded state, unfolding rate constant k_u and k_f, respectively. Briefly, calculation of the force applied by OPFC can be described in the following steps:

1. Steady-state fluorescence measurement to determine the K_{eq}

The equilibrium reaction constant K_{eq} can be measured by a steady-state temperature dependent fluorescence measurement of the DNA hairpin structure or a molecular beacon structure which contain the identical region of DNA hairpin stem-loop. At each temperature, K_{eq} of DNA hairpin stem melting is expressed as equation below, where f is the fraction of hairpins in the open state:

$$K = \frac{[open]}{[closed]} = \frac{k_u(0\ pN,T)}{k_f(0\ pN,T)} = \frac{f}{1-f} \qquad (3)$$

2: Pump-probe temperature-jump measurement to determine the k_r (0 pN, T)

The T-jump is a relaxation method where a shift in temperature acts as a perturbation. A transient temperature pump is applied and shifts the equilibrium position of the system. Then, then the dynamic change of the system can be detected by a time-resolved probe beam. Specifically, in our pump-probe setup, the time-resolved fluorescence signal was collected by a PMT and fitted to a single-exponential function. From the fitting, the relaxation lifetime (which is equal to $1/k_r$) τ_r(0 pN, T) at each temperature was extracted. The relaxation rate following the perturbation (k_r(0 pN, T)=1/τ_r(0 pN, T)) is defined as the sum of the unfolding rate k_u(0 pN, T) and the re-folding rate k_f (0 pN, T):

$$k_r(0\ pN, T) = 1/\tau_r(0\ pN, T) = k_u(0\ pN, T) + k_f(0\ pN, T) \qquad (4)$$

3:Calculation of k_u(0 pN, T) and k_f(0 pN, T)

From steps 1&2, the k_u(0 pN, T) and k_f(0 pN, T) were calculated and expressed as:

$$k_u(0\text{ pN, T}) = \frac{1}{\tau_r(0\text{ pN,T})} \times \frac{K_{eq}}{1+K_{eq}} \qquad (5)$$

and

$$k_f(0\text{ pN, T}) = \frac{1}{\tau_r(0\text{ pN,T})} \times \frac{1}{1+K_{eq}} \qquad (6)$$

4. Calculation of rate constants k_u(0 pN, T) and k_f(0 pN, T) at low temperature (T_{final} < 45°C)

Because the time-resolved T-jump with T_{final} < 45ºC did not show significant fluorescence signal across the measured timescale, it is not possible to directly measure k_r or calculate the k_u(0 pN, T) and k_f (0 pN, T) at these temperatures. In order to quantify the k_u and k_f, at these temperatures we constructed an Arrhenius plot with the unfolding rate k_u at high temperature (T_{final} ⩾45°C) and extrapolated it to the low temperature regime (T_{final} < 45°C) as shown in **Figure 3e.** The Arrhenius plot was fitted by a linear fitting function: ln(k_u(0 pN, T))= 100.07-30242.57*(1/T). From the extrapolation, ln(k_u(0 pN, 45°C)) = 5.017 and k_u(0 pN, 45°C) = 151 s^{-1}. To validate this fitting and the unfolding rate from the extrapolation, we compared the k_u(0 pN) to the reported values at 23°C for similar structure from Woodside and colleagues [9]. Importantly, because the k_u(0 pN) is temperature dependent, we further extrapolate the Arrhenius plot to 23°C and get k_u(0 pN, 23°C) = exp(-2.04) = 0.13 s^{-1}. This number agrees with the reported value k_u(0 pN, 23°C) = exp(-4.1) = 0.017 s^{-1} from a similar DNA structure (10R50/T4) with 10-mer stem with 50% GC content and 4-nt loop (GAGTCTCCTA-TTTT-TAGGAGACTC). Note that the unfolding rate of our DNA structure is greater than the reported values for other stem loop hairpins. This is likely due to the low GC content (~22%) in our stem, different experimental conditions (200 mM monovalent salt in Woodside's paper and 5 mM Tris-HCl, 10 mM $MgCl_2$ and 1 mM EDTA in our work), and the shorter loop (7 in our work compared to 4 nt loop used by Woodside et al.). Accordingly, the folding rate k_f (0pN) at low temperature can be calculated using the K_{eq} from the steady-state measurement in step 1: $k_f(0\text{ pN, T}) = \frac{K_{eq}}{k_u(0\text{ pN,T})}$

5. Pump-probe force-jump measurement to determine the k_r (F, T)

Similar to the T-jump measurement for the DNA hairpin, the relaxation lifetime τ_r(F, T) was acquired from single exponential fitting of the time-resolved fluorescence signal. The relaxation rate under force k_r (F, T)=1/τ_r(F, T), is defined as the sum of the unfolding rate k_u(F, T) and folding rate k_f(F, T) with the application of force.

$$k_r(\text{F, T}) = 1/\tau_r(\text{F, T}) = k_u(\text{F, T}) + k_f(\text{F, T}) \qquad (7)$$

6. Estimation of the force

We next calculated the force using the Bell model which was first developed by G. Bell in 1978 [10]. The Bell model predicts how forces modulate the kinetics of an idealized two-state system separated by a single barrier under constant force. In the Bell model, the force effectively modulates the k_u and k_f as follows [10]:

$$k_u(F,T) = k_u(0\,pN,\mathrm{T}) \times \exp\left(\frac{F\Delta x_u{}^{\ddagger}}{\mathrm{k_B T}}\right) \qquad (8)$$

$$k_f(F,\mathrm{T}) = k_f(0\,pN,\mathrm{T}) \times \exp\left(\frac{-F\Delta x_f{}^{\ddagger}}{\mathrm{k_B T}}\right) \qquad (9)$$

$\Delta x_u{}^{\ddagger}$ and $\Delta x_f{}^{\ddagger}$ are the distance to the transition state. Previously, Woodside's work reported experimental measurement and theoretical estimation of $\Delta x_u{}^{\ddagger}$ of the similar DNA hairpin sequence ($\Delta x_u{}^{\ddagger}$ = 4.0 nm, $\Delta x_f{}^{\ddagger}$ = 5.1 nm, 10R50/T4)[9].

From step 5, the relaxation time of force-jump experiment can now be written as:

$$k_r(\mathrm{F,T}) = \frac{1}{\tau_r(\mathrm{F,T})} = k_u(0\,pN,\mathrm{T}) \times \exp\left(\frac{F\Delta x_u{}^{\ddagger}}{\mathrm{k_B T}}\right) + k_f(0\,pN,\mathrm{T}) \times \exp\left(\frac{-F\Delta x_f{}^{\ddagger}}{\mathrm{k_B T}}\right) \qquad (10)$$

Therefore, the only unknown variable, force (F) can be calculated. At 45℃, we calculated the effective force generated by the OPFC is 3.4 ± 0.45 pN from triplicate measurements of the F-jump and T-jump experiments (**Figure S11&12**).

Note S3. OxDNA simulation
OxDNA Model

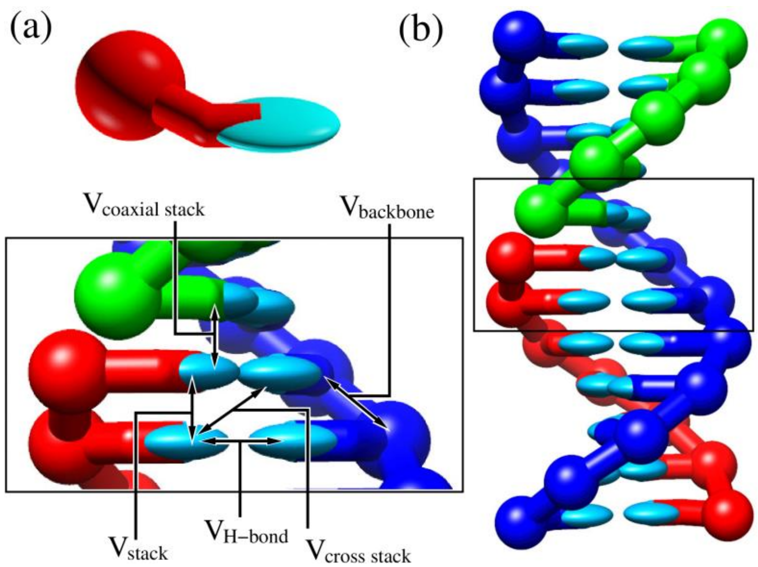

Note Figure S1: (a) A representation of a rigid oxDNA nucleotide. (b) A 12-base-pair DNA double helix as represented by oxDNA. The inset shows the different types of interactions that are accounted for in the oxDNA model, namely, hydrogen-bonding between complementary bases, (coaxial) stacking interactions between bases, cross-stacking interactions between diagonally-opposite bases in a double helix, and a FENE potential between backbone sites, as well as excluded-volume repulsions associated with the backbone and base sites.

OxDNA is a coarse-grained model simulation of DNA at the nucleotide level [11-13]. **Note Figure S1** shows a double helix as represented by oxDNA with the interactions that contribute to the model illustrated. The parameters of the model have been fitted to reproduce the structure, thermodynamics and mechanics of double-stranded and single-stranded DNA with a particular focus on the thermodynamics of hybridization. We use the second-generation version of the oxDNA model (sometimes called "oxDNA2") introduced by Snodin et al. [13]; this included changes that improved the description of large DNA nanostructures such as origamis. OxDNA's excellent reproduction of the structure of DNA origamis has been further confirmed by a detailed comparison to a high-resolution origami structure obtained by cryoEM [14-15]. Consequently, it has been widely used to model the structure of DNA origamis with much success. Particularly relevant to the current application is oxDNA's ability to describe the mechanical properties of origamis, because of the tensile forces applied by the linkers and hairpins to the origami force clamp. Importantly, it has been shown to provide a reasonable description of both the elastic moduli of DNA origamis [16] and the local unravelling of DNA origami through unbinding of staple domains due to applied tension [17]. Note, that the tensile forces were found to be not sufficiently large to cause any staple unbinding in the case of the OPFC. Also important to the current application is oxDNA's ability to capture the effects of tension on small DNA motifs, such as hairpins and duplexes [18-19]. This stems from its good description of the thermodynamics of hybridization and hairpin formation [11], the force-extension curves of single-stranded DNA [12] and the persistence length of double-stranded DNA [11, 13]. For all these reasons oxDNA is particularly well-suited to describe the OPFC. Similarly, it has also been used to calibrate the origami force sensor [20] of Nickels *et al.* [21].

System setup

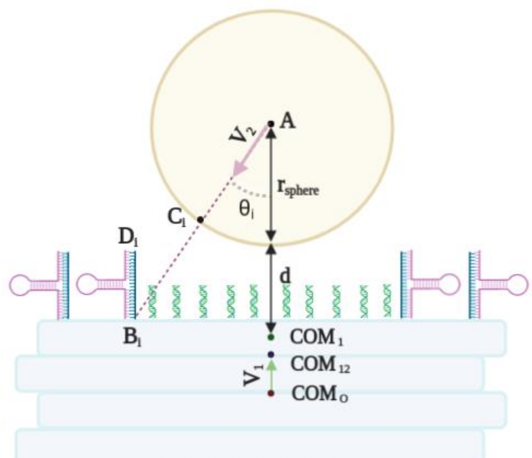

Note Figure S2: Schematic to show how the parameters for modelling the polymer sphere in the oxDNA simulations are chosen (for clarity only two of the three hairpins on each side are shown). The relative sizes of the objects are not to scale.

In the oxDNA simulations we do not model the sphere explicitly, but instead model it effectively by a set of harmonic traps that constrain the positions of the end nucleotides that are attached to the polymer sphere. These traps lie on the surface of a sphere with a radius appropriate for the given temperature. **Note Figure S2** illustrates our approach for calculating the positions of the traps at low temperature. First, we calculate the centers of mass of the origami (**COM_O**), its top layer (**COM_1**) and its two top-most layers (**COM_{12}**). From the center of the top layer, we then added a vector of magnitude ($d + r_{sphere}$) in the direction given by the vector **$V_1 = COM_{12} - COM_O$** to get the center of the sphere (**A**). We assume that the hairpins/linkers are attached to the closest point on the polymer sphere. The details are as follows. For each linker/hairpin, we define their point of attachment **(B_i)** to the origami based on an equilibrated origami configuration; we then define the vector $\mathbf{V_2} = \mathbf{B_i} - \mathbf{A}$ for each linker/hairpin. In the direction of $\mathbf{V_2}$ we add a vector of magnitude r_{sphere} to $\mathbf{A}$ to get $\mathbf{C_i}$ the trap center for that particular linker/hairpin that represents its attachment to the sphere. To calculate the trap positions for the sphere $\mathbf{C_i}$ at high temperature, we assumed that the sphere underwent a uniform contraction, keeping the angle (θ_i) the same but decreasing r_{sphere} from 280 nm at 313 K to 205 nm at 328 K. After all the trap centers are calculated for the linkers and hairpins, the origami is simulated at 313 K and 328 K until the hairpins have reached the required distance from the center of the sphere and the forces have equilibrated.

Simulation details

$\mathbf{L_{110nm}}$ is our initial model system, with the six hairpins located at the two extremes of the origami in groups of 3. To investigate the effect of the position of the hairpins on the origami on the force exerted by the sphere, we simulated five more systems ($\mathbf{L_{90nm}}$ - $\mathbf{L_{10nm}}$) where the hairpins were progressively moved to the center of the origami. $\mathbf{L_{10nm}}$ had all the hairpins concentrated at the center of the origami. The **Δ32** system had the hairpins in the same position as $\mathbf{L_{110nm}}$ but lacked multiple staple strands at the center of the origami. The absence of staple strands makes **Δ32** much more flexible than the other origamis. We assume the sphere to have a radius of 280 nm at 313 K and 205 nm at 328 K. We perform MD simulations to simulate each system at 313 K and 328 K in the canonical *NVT* ensemble[22]; we will refer to these as the low and high temperature states. The coupling between the system and a heat bath is emulated by employing an Andersen-like thermostat [23]. We chose harmonic traps with a force constant of 28.545 pN/nm to model the effect of the sphere and run our simulations until the forces have equilibrated. The only difference between the high and the low temperature states is the radius of the polymer sphere. At low temperature, the trap positions on the sphere are closer to the respective hairpins and linkers, and consequently the force felt is low. At high temperature, the sphere shrinks, and the trap positions all move towards the center of the sphere thereby increasing the distance between them and the hairpins and linkers which results in larger forces. The forces experienced by the origami at high temperature has a compressive component as well as a lateral bending component because of the sphere shrinkage. We also perform simulations at high temperature with "mutual traps" between the nucleotides in the hairpin so that the hairpins are prevented from unfolding, thus allowing us to obtain the forces experienced in the absence of any hairpin unravelling.

Assumptions

There are a number of assumptions in the setup of the simulations of which it is important to be aware. First, we assume that when the hairpins and linkers attach to the polymer sphere (in the low temperature regime for the sphere size) they attach to the closest point on the polymer spheres, which we assume are perfectly smooth. In practice, although this is a reasonable assumption for the average position of the attachment points across the ensemble of origamis, we expect there to be a distribution of such points across the ensemble of origamis. We do not account for this potential heterogeneity in population of the OPFCs. Second, we do not explicitly account for the elastic mechanical properties of the sphere. For example, the spring constant for our harmonic traps is in the "stiff-sphere" limit where the obtained forces do not depend on the spring constant because the origami is more compliant than the traps. Third, we assume that all the hairpins and linkers are simultaneously attached to the sphere. The parallel application of the forces through all these linkers and hairpins is the reason for the significant bending of the origami. If not all linkers/harpins are bound, then the total applied force on the origami is likely to be less and the origami less bent, which in turn is likely to lead to higher forces through the hairpins/linkers that are attached.

We also note that upon close inspection that the 16HB origami has an inherent twist of around -80° between the two ends. Such twist is expected for an origami based on a square lattice of helices without insertions or deletions [24]. However, this twist is too low to have significantly affect the geometric assumptions of the design.

Further results.

System	T = 313 K	T = 328 K
L_{10nm}	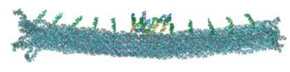	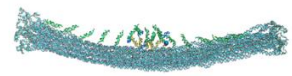
L_{30nm}	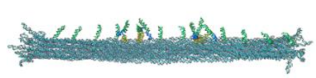	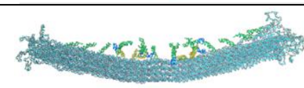
L_{50nm}	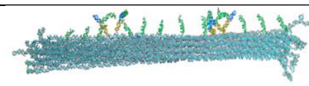	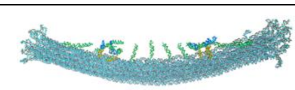
L_{70nm}	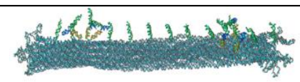	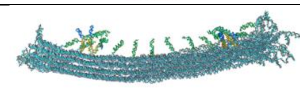
L_{90nm}	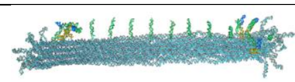	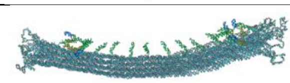
L_{110nm}	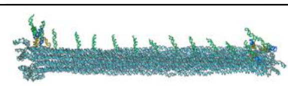	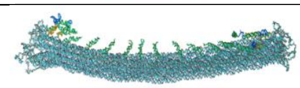
$L_{110nm}(\Delta 32)$	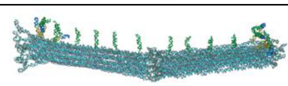	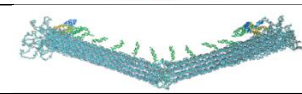

Note Figure S3: Snapshots of C1-C6 and Δ32 at low and high temperatures. At high temperature, a strong bend is visible in all C1-C6 while Δ32 is kinked.

Configurations for each of the origami force clamps are illustrated in **Note Figure S3** at both low and high temperature. The combined effect of the forces on the hairpins and linkers causes the origami to bend significantly. Although, the force acting through each individual hairpin/linker is not particularly high, the sum of all such forces is substantial. At low temperature, we note that all the hairpins and linkers are roughly oriented radially towards the center of the sphere, meaning they are co-linear with the radius vector at that point on the sphere. We note from the average forces that as the sphere shrinks, the hairpins and linkers in the center of the origami tend to be in a state of compression rather than tension because of their proximity to the surface of the sphere. At high temperature, the origami bends more as a result of the higher average force exerted on the system. The average bending is more for $\mathbf{L_{10nm}}$ than $\mathbf{L_{130nm}}$ because of the tension in the outer linkers in $\mathbf{L_{10nm}}$ whereas in $\mathbf{L_{130nm}}$, the hairpins can also absorb the stress by unfolding. The deletion of 16 staple strands in **Δ32** gives the origami significantly more flexibility and therefore it bends more at high temperature. We observe that the average angle of bending between the two origami blocks either side of the flexible section is significantly larger at 328 K (42.616°) compared to at 313 K (13.066°) because the origami has deformed to absorb much of the strain due to the particle collapse, thereby making hairpin unfolding much less likely (**Table S1**).

Table S1: Average angle of origami bending and standard error along hairpins.

Configuration	Angle of bending at 313 K (º)	SEM (º)	SD (º)	Angle of bending at 328 K (º)	SEM (º)	SD (º)
L_{10nm}	4.386	0.04933	2.20613	26.081	0.05646	2.52491
L_{30nm}	4.095	0.05956	2.34862	24.777	0.05616	2.51142
L_{50nm}	3.033	0.03746	1.67528	22.152	0.06766	2.62741
L_{70nm}	3.506	0.04647	1.82597	20.742	0.06157	2.75349
L_{90nm}	3.315	0.04069	1.66616	18.904	0.0682	2.5307
L_{110nm}	3.849	0.046	1.81929	23.865	0.0474	2.11963
$L_{110nm}(\Delta 32)$	13.066	0.1544	6.90483	42.616	0.0788	3.52405

Measurement of forces

The forces transmitted through the hairpins and linkers can be measured through the forces exerted by the traps modelling their attachment points to the sphere. These traps are harmonic, and so forces they exert have the form $\mathbf{F} = -k(\mathbf{r} - \mathbf{r_0})$ where **F** is the instantaneous force, *k* is the spring constant or stiffness, **r** is the position of the nucleotide at that instant and $\mathbf{r_0}$ is the equilibrium position of the trap. If **F** is the total force acting on a nucleotide at any instance, the force through the hairpin is measured by defining a component of this force $\mathbf{F}_{||}$ which acts along the direction given by the vector $\mathbf{V_3} = \mathbf{B_i} - \mathbf{D_i}$ where $\mathbf{D_i}$ is the position of the top-most nucleotide in that strand (the nucleotide on which the trap force is being applied). So, we have:

$$\mathbf{F}_{||} = \mathbf{F} \cdot \frac{\mathbf{V_3}}{||\mathbf{V_3}||}$$

We can say that if $\mathbf{F}_{||} > 0$, the linker/hairpin is under tension and if $\mathbf{F}_{||} < 0$, the linker/hairpin is under compression. **F** and $\mathbf{F}_{||}$ were measured at low and high temperatures for each hairpin and they were plotted along with their moving averages (calculated using 11 data points in the neighborhood of a particular data point). The force acting along the hairpins averaged over all configurations and all hairpins in the system is given in **Table S2**.

Table S2: Average force and standard error along hairpins (n = 6)

Configuration	Force along hairpins at 313 K (pN)	SEM (pN)	SD (pN)	Force along hairpins at 328 K (pN)	SEM (pN)	SD (pN)
L_{10nm}	-0.176	0.723	1.772	-0.628	0.246	0.603
L_{30nm}	-0.063	0.829	2.031	-0.402	0.415	1.016
L_{50nm}	-0.229	0.644	1.577	-0.075	0.588	1.441
L_{70nm}	-0.126	0.686	1.681	0.716	0.809	1.982
L_{90nm}	-0.101	0.709	1.737	2.609	2.035	4.985
L_{110nm}	0.310	0.965	2.364	4.457	1.847	4.524
L_{110nm} $(\Delta 32)$	-0.247	0.344	0.842	1.264	1.035	2.534

We note that there are fast fluctuations in the instantaneous force due to the trapped nucleotides oscillating around their average position in the trap center; thus, the force distribution is quite wide. At low temperature, we do not observe any of the hairpins breaking. Under high temperature conditions, some of the hairpins break which can be attributed to both thermal and mechanical effects. We clearly observe a trend in hairpin unfolding based upon the position of the hairpin on the origami. The hairpins close to the center of the origami ($\mathbf{L_{10nm}}$) feel the least tension and the ones towards the extremes ($\mathbf{L_{110nm}}$) feel the most tension. From **Table S1** it is clear that none of the systems have hairpins under strong tension at 313 K. At 328 K, only hairpins of $\mathbf{L_{110nm}}$ experience tension comparable to their $\mathbf{F_{1/2}}$ (~4.8 pN). When "mutual traps" are placed onto the hairpin nucleotides, they are unable to break and relieve any of the tension. This leads to a small increase in the average force for the systems with hairpins far apart (mainly $\mathbf{L_{90nm}}$ and $\mathbf{L_{110nm}}$).

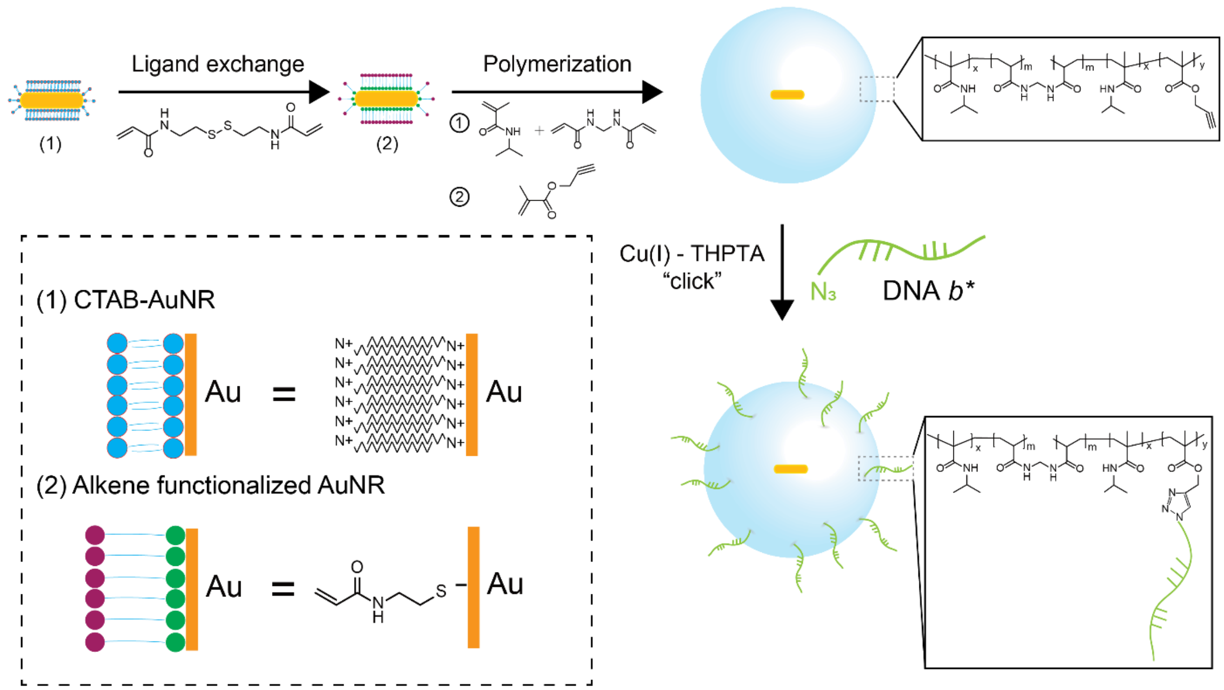

Figure S1. Synthesis of pNIPMAm particle. First, the CTAB-gold nanorod was decorated with an alkene function group (N, N'-bis(acryloyl)cystamine) via ligand exchange. The polymer shell was then built by polymerization of 0.1g N-isopropylmethacrylamide and 0.01 g of the crosslinking agent N,N'-methylenebisacrylamide at 70°C for 2 hr. The alkyne functional group was introduced via dropwise injection of 0.01 ml of propargyl methacrylate monomer. DNA anchor was then incorporate on the particle surface via copper-free click chemistry.

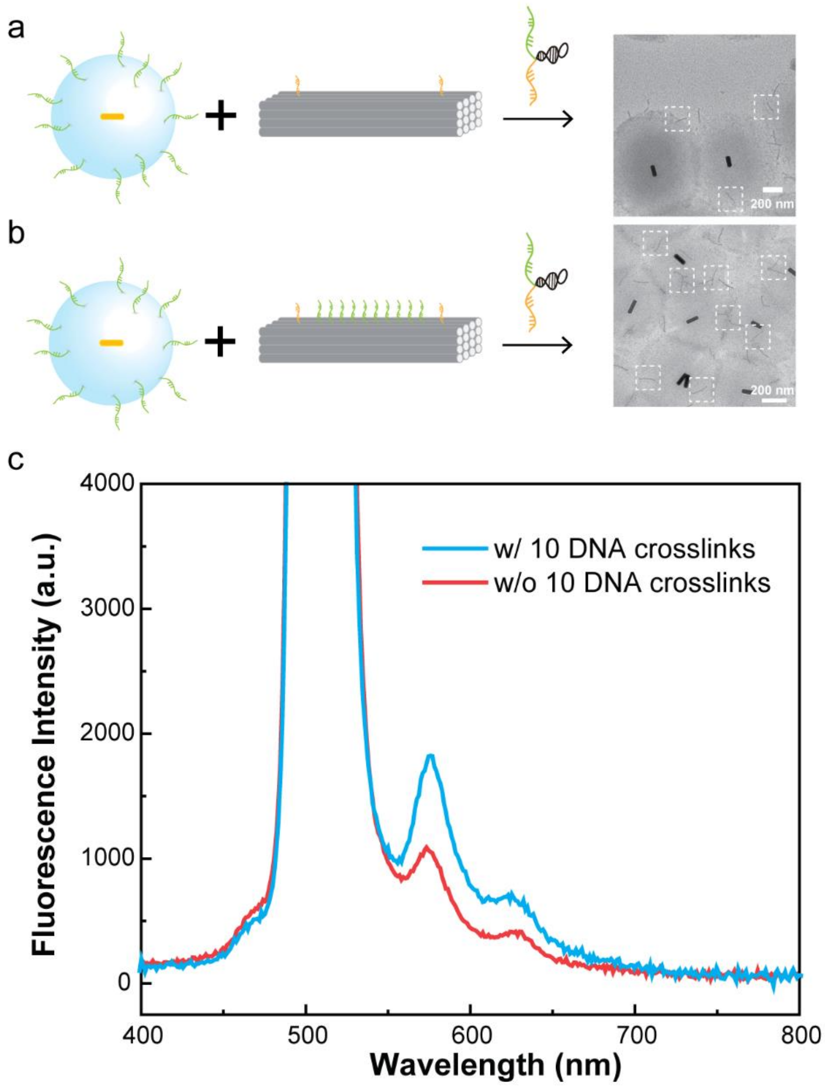

Figure S2. Validating the specificity of DNA-guided OPFC assembly. Schematic and TEM images (**a-b**) along with fluorescence spectra demonstrating the importance of the 10 DNA crosslinks in boosting the yield of OPFC assembly. The data is representative from two replicates. To reduce the cost of DNA hairpin and origami that were used in replicates, only two hairpins were incorporated on the origami and the particle and DNA origami were mixed in a lower concentration than other OPFC experiments in this work. Fluorescence spectra of nearly identical samples prepared by mixing 8 µl of 0.6 nM polymer particles with 50 µl of 9 nM origami beam and allowed to hybridize overnight at room temperature. The sample was then washed 5 times (5000 rpm, 6 mins, in 5 mM Tris-HCl, 10 mM $MgCl_2$ and 1 mM EDTA at pH = 8) by centrifugation and redispersed for experiments. The fluorescence spectra in (**c**) were collected using a 520 nm excitation wavelength that was selected to excite the Cy3B dye while also providing some spectral separation from the strong scattering generated by the responsive particles. The Cy3B emission peak was at 575 nm and its intensity indicates the yield of OPFCs assembled with origami beams.

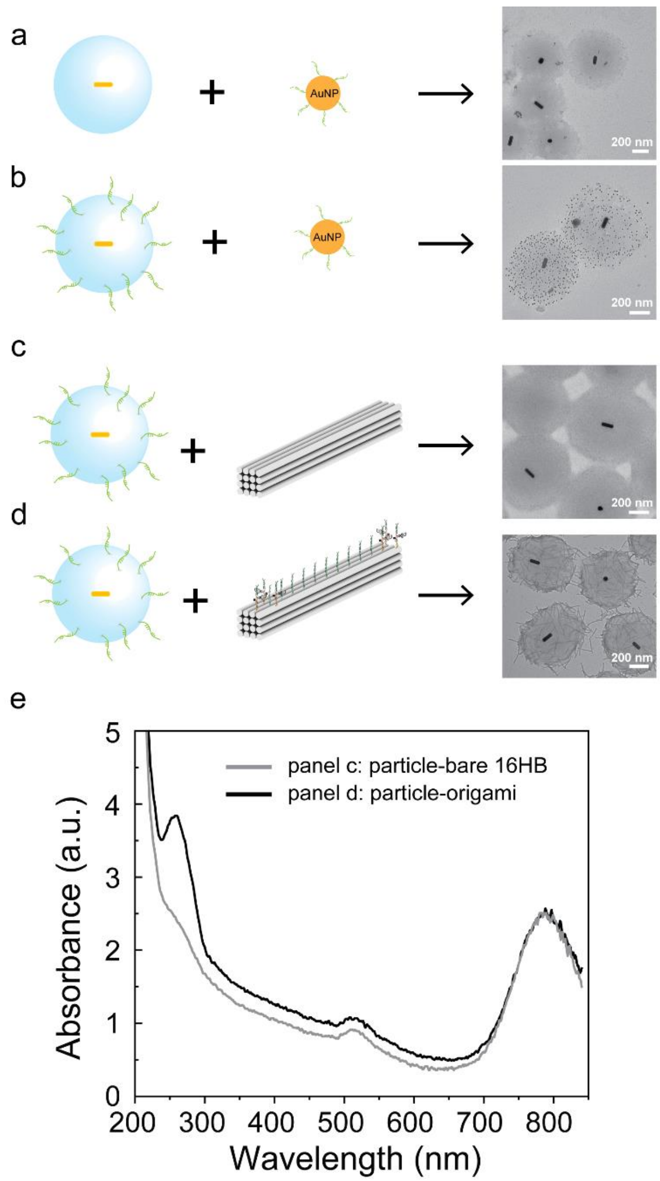

Figure S3. Characterization and validation of DNA-mediated OPFC assembly. (**a-b**): Schematic and TEM images of pNIPMAm particles with/without DNA handles (b-b*) incubated with DNA coated AuNPs. (**c-d**): Schematic and TEM images of pNIPMAm particles incubated with 16HB DNA origami loaded with/without target molecules. (**e**): Absorbance spectra of panel c and d confirms DNA-mediated assembly of OPFC. Absorbance spectra were collected using NanoDrop 2000 (Thermo Scientific) from 200 nm to 850 nm. Samples were prepared by mixing 15 µl of 0.3 nM of polymer particles with 50 µl of 30 nM origami beam or 50 µl of ~ 1 nM 13nm lab-synthesized gold nanoparticles and allowed to hybridize overnight at room temperature. The sample was then washed 5 times (5000 rpm, 6 mins, in 5 mM Tris-HCl, 10 mM $MgCl_2$ and 1 mM EDTA at pH = 8) by centrifugation and redispersed in 40 µl buffer B (5 mM Tris-HCl, 10 mM $MgCl_2$ and 1 mM EDTA at pH = 8) and measured shortly after sample preparation.

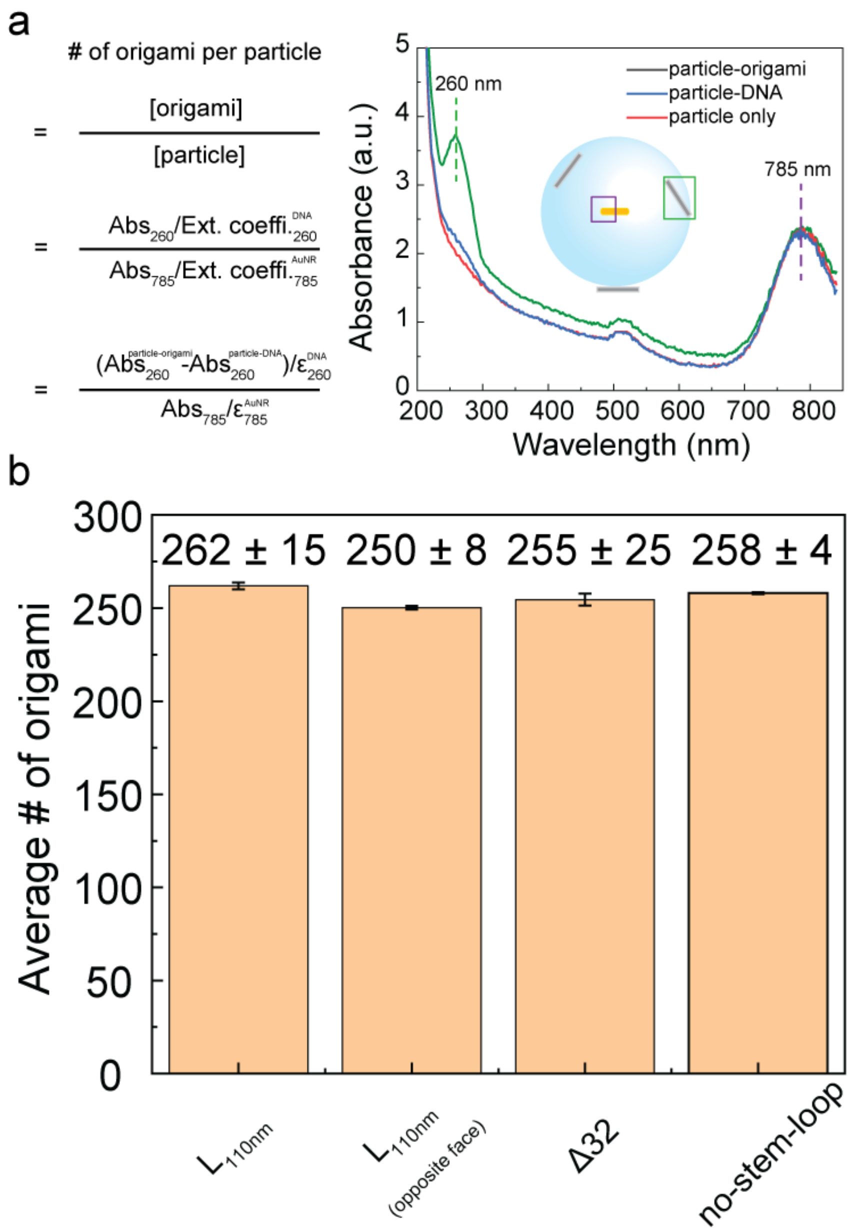

Figure S4. Quantification of origami beam number on polymer particles. (a) Absorbance spectroscopy of OPFC and controls. Stoichiometry between origami and particle is quantified using the extinction coefficient of the AuNR core within each OPFC ($\varepsilon_{785\ nm} = 3.7\text{x}10^{10}\ M^{-1}cm^{-1}$) and the origami ($\varepsilon_{260\ nm} = 1\text{x}10^{8}\ M^{-1}cm^{-1}$). Absorbance at 260 nm (Abs_{260}) was corrected by subtracting the absorbance at 260 nm of particle-DNA (blue curve, $Abs_{260}^{particle\text{-}DNA}$) from particle-origami sample (green curve, $Abs_{260}^{particle\text{-}origami}$). (**b**) Plots of origami beam copy number on each OPFC in different OPFC designs. Error bars represent the standard deviation from three independent measurements. Samples were prepared as described in **Figure S3**. 2 µl of each sample was added to NanoDrop 2000 spectrophotometer for absorbance measurement.

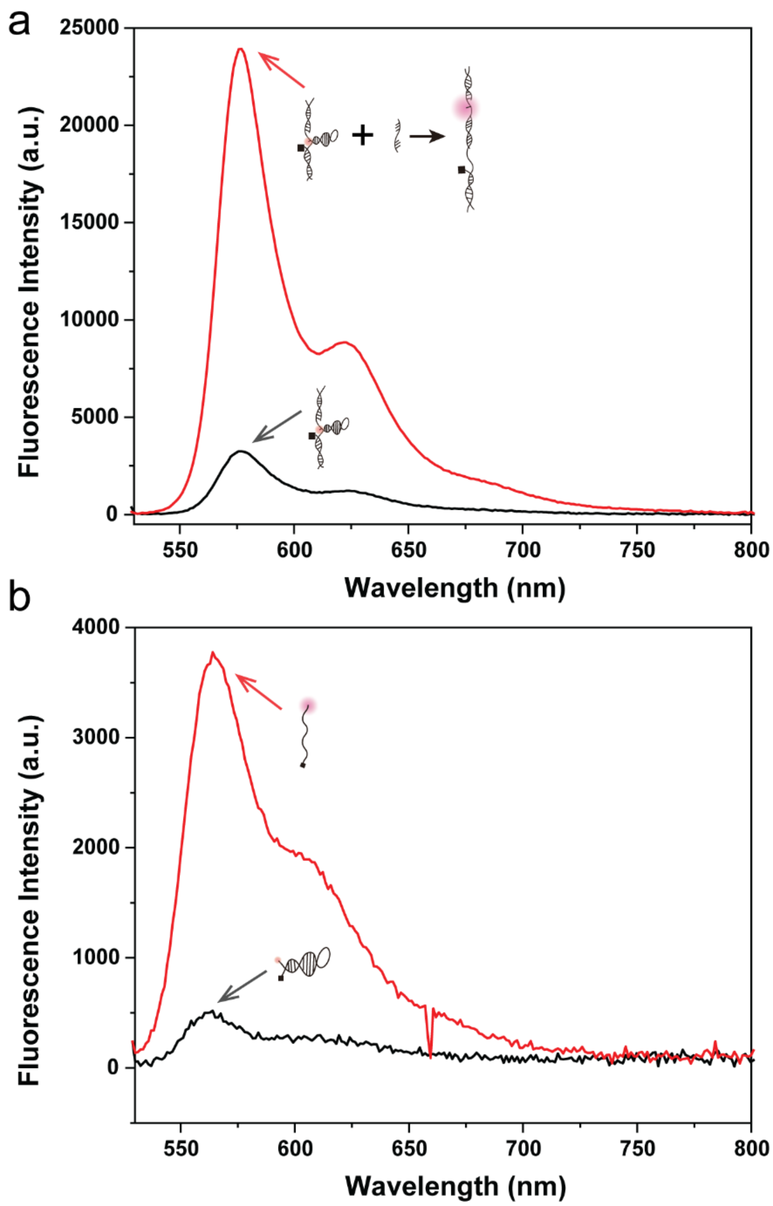

Figure S5. Fluorescence measurements of DNA hairpin in folded and extended states. (**a**) Spectra showing the fluorescence intensity of DNA hairpin before (black) and after (red) hybridizing to a 17mer short oligonucleotide (sequence shown in **Table S1**). The fluorophore (Cy3B) and quencher (QSY9) pair positioned on complementary strands of the hairpin. To unfold the DNA hairpin, 150 nM of DNA hairpin was hybridized with 1.5 µM 17mer complementary DNA for 3hr at room temperature. (**b**) Spectra showing the fluorescence intensity of hairpins lacking the arms and only including the stem region before (black, 20°C) and after (red, 70°C) thermal melting. The fluorophore (Cy3) and quencher (QSY9) pair positioned at the two ends of the hairpin. Both samples were prepared and measured at 150 nM in Buffer B (5 mM Tris-HCl, 10 mM $MgCl_2$ and 1 mM EDTA at pH = 8) and measured shortly after sample preparation. The significantly different maximum intensity between **a** and **b** is likely due to the different quantum yield of Cy3B and Cy3. (Cy3B is reported having ~8 fold greater fluorescence compared to Cy3 at equimolar concentration [25])

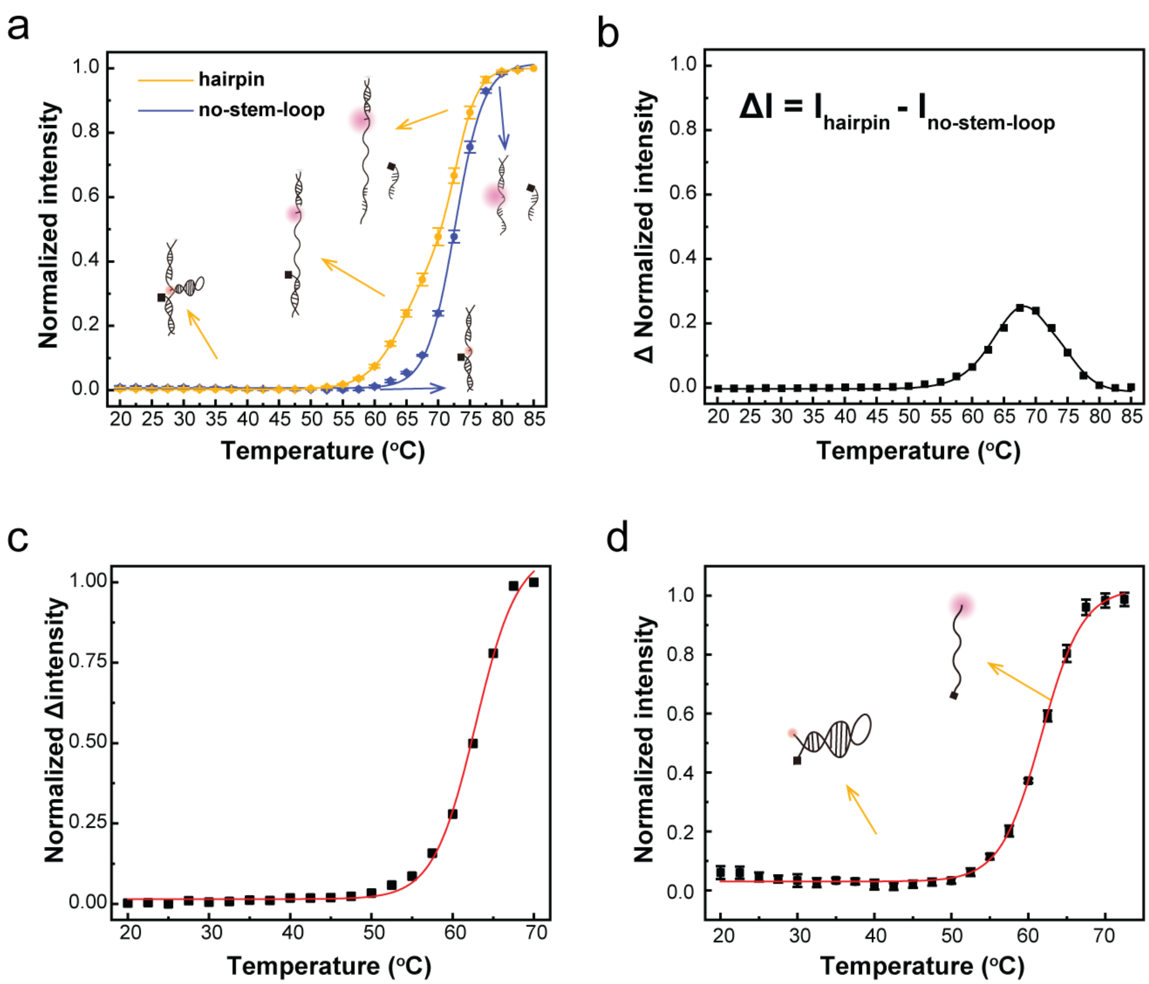

Figure S6. Thermal melting profile of target DNA hairpins. (**a**) Temperature-dependent fluorescence intensity of DNA hairpin and control lacking the stem-loop domain. The blue represents a control lacking the stem-loop while the yellow corresponds to the standard 4.7 pN hairpin used throughout this study. The increase in fluorescence is due to both the stem melting as well as arm melting, and these two transitions are overlapping with stem T_m = 64°C and arm T_m = 72°C. Error bars correspond to the standard deviation of triplicate measurements. (**b**) Fluorescence intensity difference between hairpin and no-stem loop control as measured from the thermal melting experiments. (**c**) A normalized plot using the data from panel **B** in the range from 20°C to 70°C. (**d**) Temperature-dependent fluorescence intensity of DNA hairpins identical to the one studied through this work but lacking the arms. The T_m here was = 62°C confirming minimal contribution from the arms. For all these measurement, [DNA] = 150 nM and the hairpin was prepared from a 1:1:1 mixture of the three oligonucleotides comprising the hairpin probe. Measurements were performed in Buffer B (5 mM Tris-HCl, 10 mM $MgCl_2$ and 1 mM EDTA, pH = 8).

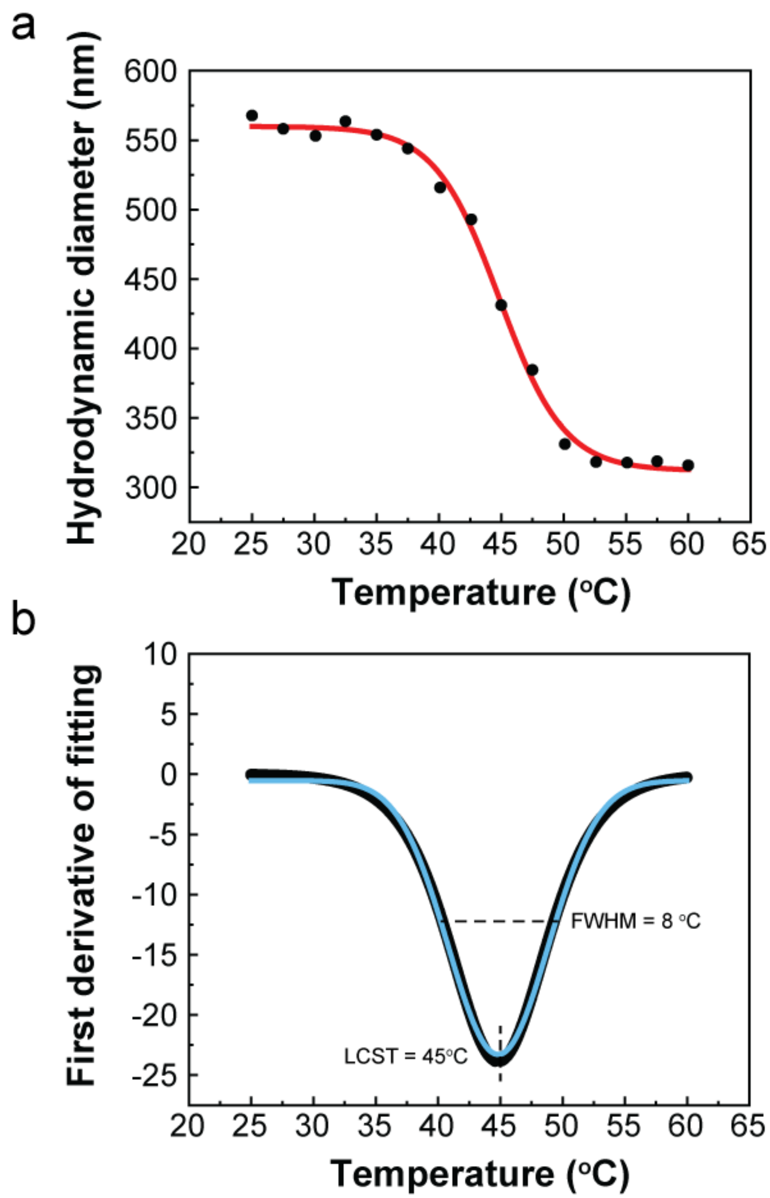

Figure S7. Characterization of transition temperature of particle actuators. (**a**) Hydrodynamic diameters of particles as a function of temperature. The data was fit with a Boltzmann sigmoid function. (**b**) Calculated first derivative of the data shown in **a**, confirming transition temperature LCST= 45°C and FWHM= 8°C.

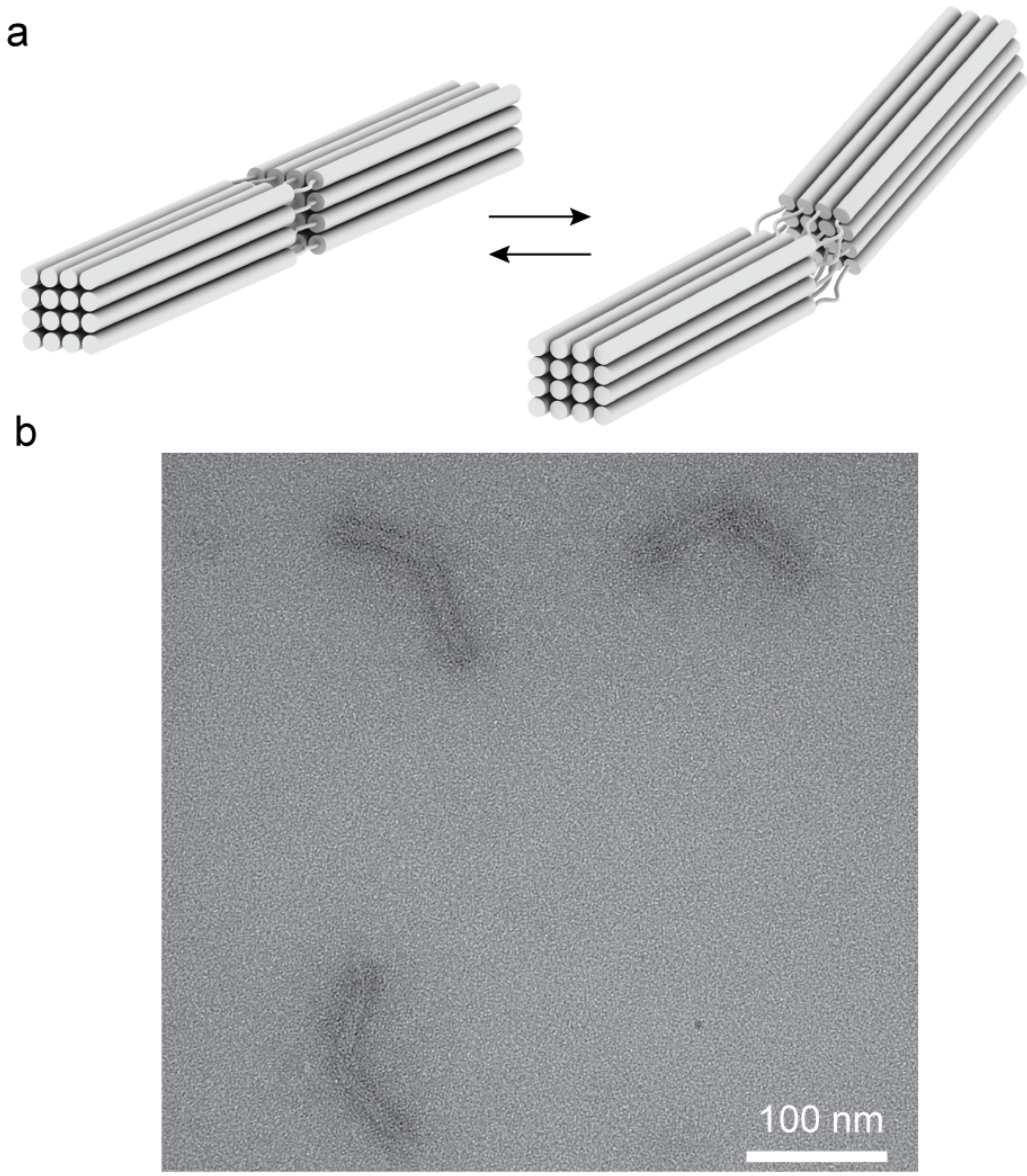

Figure S8. Design of flexible origami beams (Δ32). (**a**) Schematic showing the Δ32 origami beam. The deletion of 16 staple strands in the center of the origamis gives the structure significantly more flexibility. (**b**) Representative TEM image showing bending of Δ32 structures.

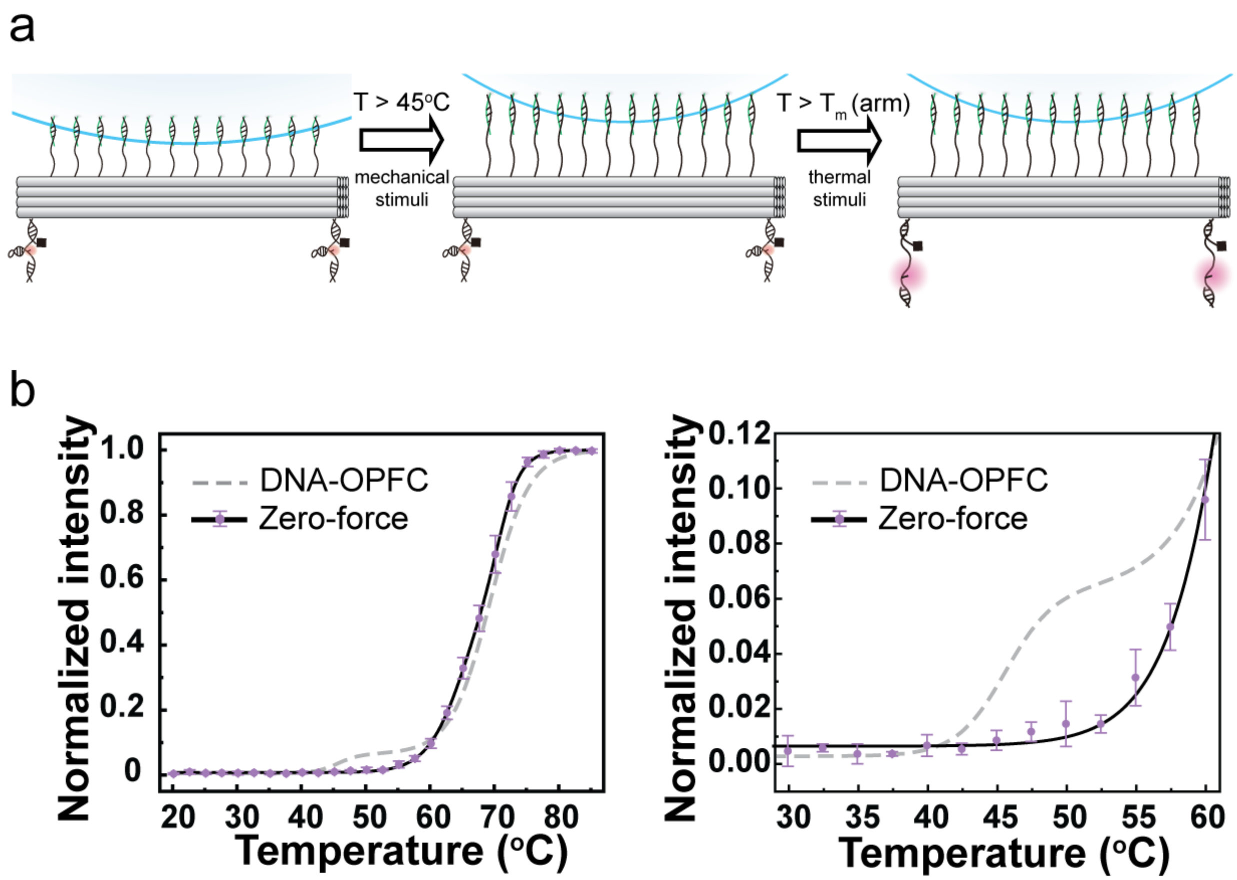

Figure S9. Zero-force control OPFC device with target hairpins located at the opposite face away from the particle actuator. (a) Schematics of zero-force control. In this experiment, we created chemically identical OPFC loaded with the same target, but with a geometric mutation. The hairpin was placed on the opposite face of the beam away from the 10 crosslinks and the particle. In this case, the collapse of the particle is not expected to generate any mechanical tension on the hairpin. (**b**) Bulk temperature-dependent fluorescence measurements of zero-force control showed no notable mechanical unfolding signal in the 45-55°C window. Samples were prepared by mixing 15 µl of 0.3 nM of polymer particles with 50 µl of 30 nM origami beam. The mixture was then washed by centrifuge and redispersed in 40 µl Buffer B as described before in the methods section. Error bars represent the standard deviation from triplicate preparations of the zero-force control OPFC. The black line is the same fit as the DNA-OPFC data shown in **Fig. 1d** (blue curve).

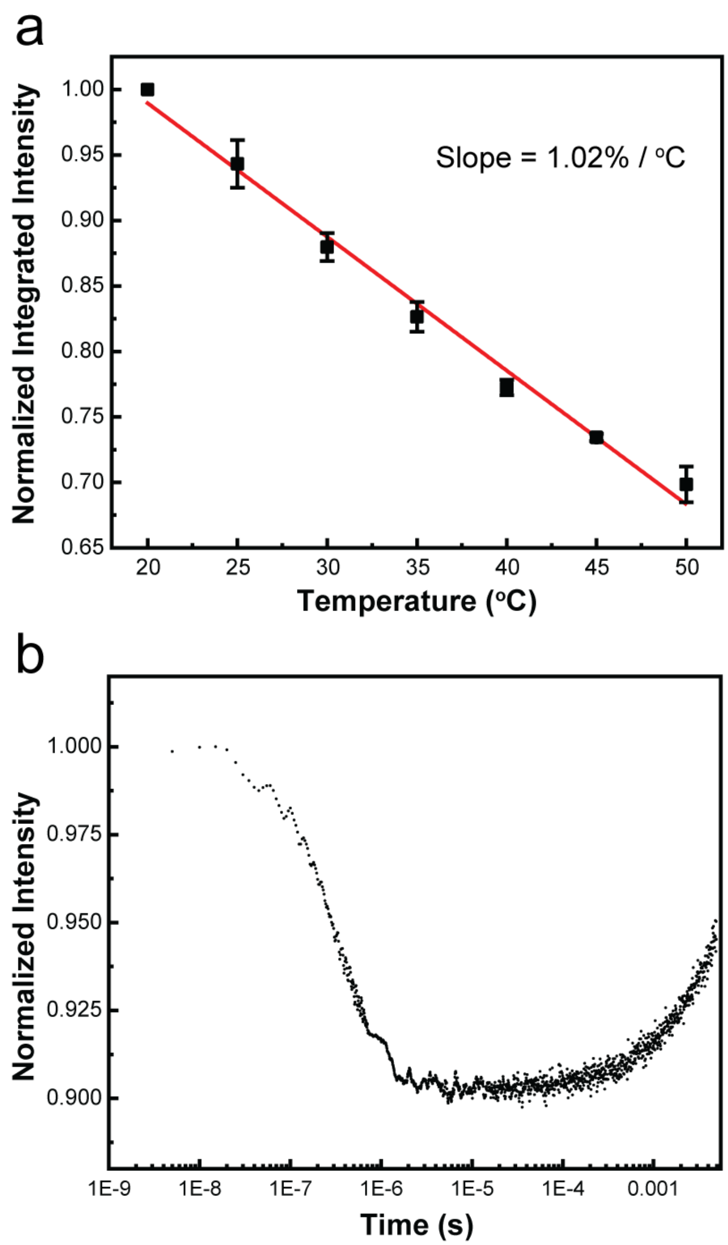

Figure S10. Temperature calibration curve of T-jump experiment with Rhodamine B standard. (**a**) Calibration curve measuring the temperature-dependent emission of Rhodamine B at a concentration = 150 nM. The temperature was ramped from 20 to 50 °C and controlled using a water bath and allowed to come to equilibrium for 5 min at each temperature. Error bars represent the standard deviation from triplicate measurements. The red line represents a linear regression to the data (Intensity = -0.0102*Temperature + 1.1038, R^2=0.9907). (**b**) Time-resolved fluorescence signal of Rhodamine B following a 10 nsec pump. The plot shows a 10% reduction of fluorescence intensity, which indicates a 10°C temperature jump, and confirms the 3 μs instrument response time.

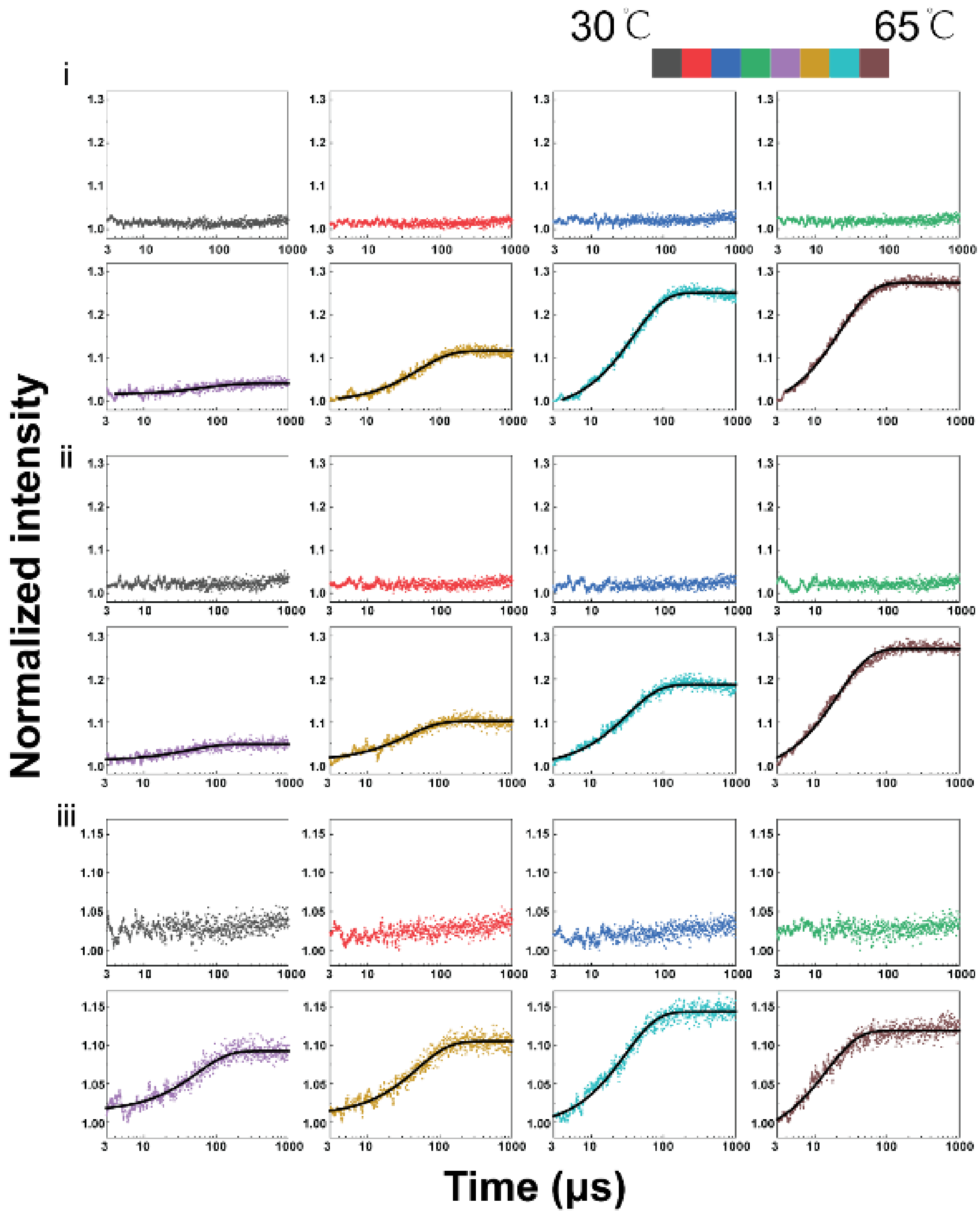

Figure S11. Spectra of T-jump experiments. Three replicates (i)-(iii) of temperature jump (ΔT = 10°C) showing transients of DNA hairpin (100 nM) thermal melting in buffer B. The data is fitted to a single exponential (black line). The colors indicate the initial temperature of the sample and ranged from 30°C to 65°C. Importantly, there was no thermal melting signal when the initial temperature was 45°C or lower. This is consistent with the bulk fluorescence data showing that the T_m of the hairpins is 64°C.

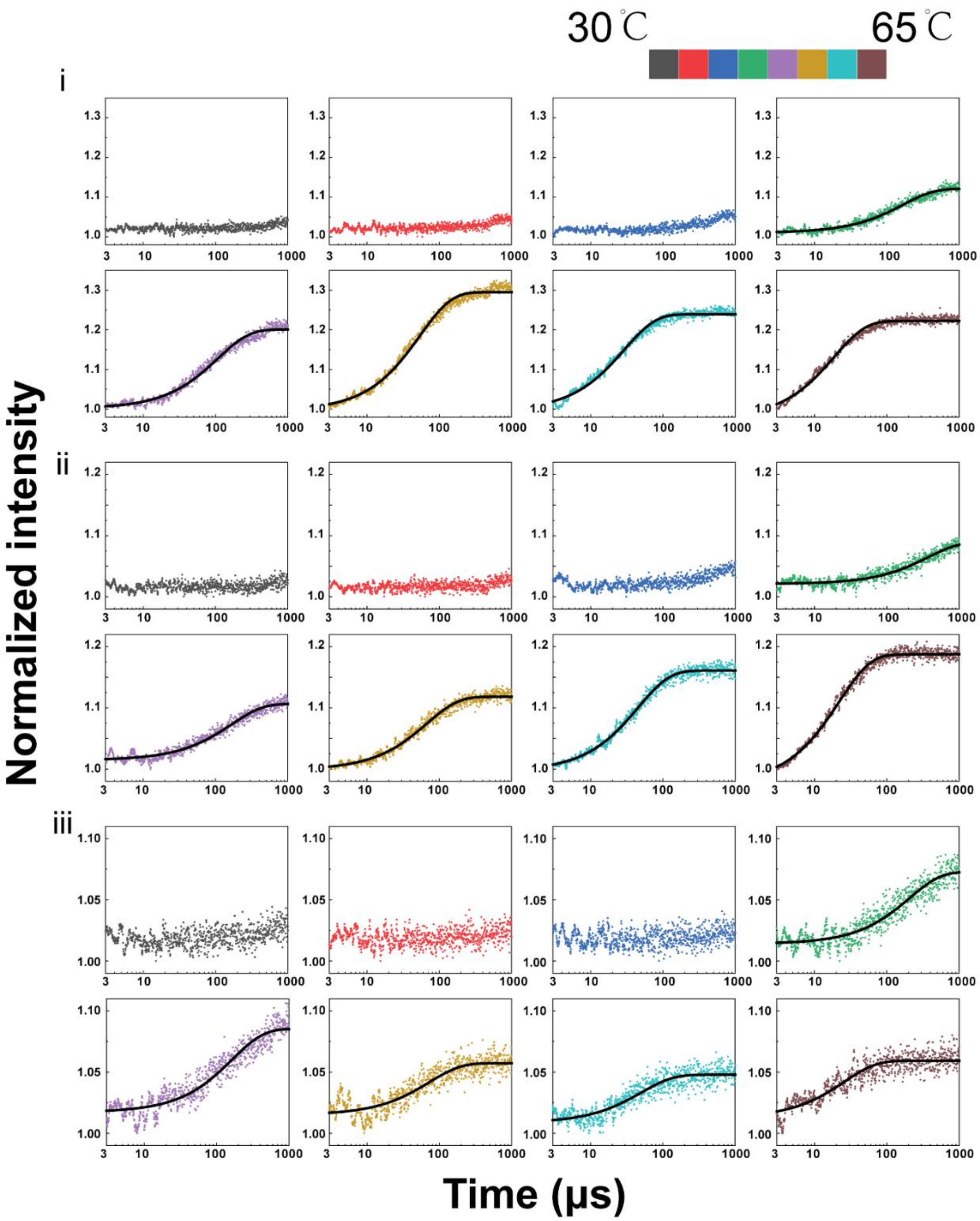

Figure S12. Spectra of F-jump experiments. Three replicates (i)-(iii) of force jump measurements (ΔT = 10°C) showing transients of mechanical unfolding of DNA hairpins (~100 nM) loaded onto the OPFC. The data is fitted to a single exponential (black line). The colors indicate the initial temperature of the sample and ranged from 30°C to 65°C. Importantly, there is now a mechanical melting signal when the initial temperature was 45°C which is consistent with the LCST of pNIPMAm.

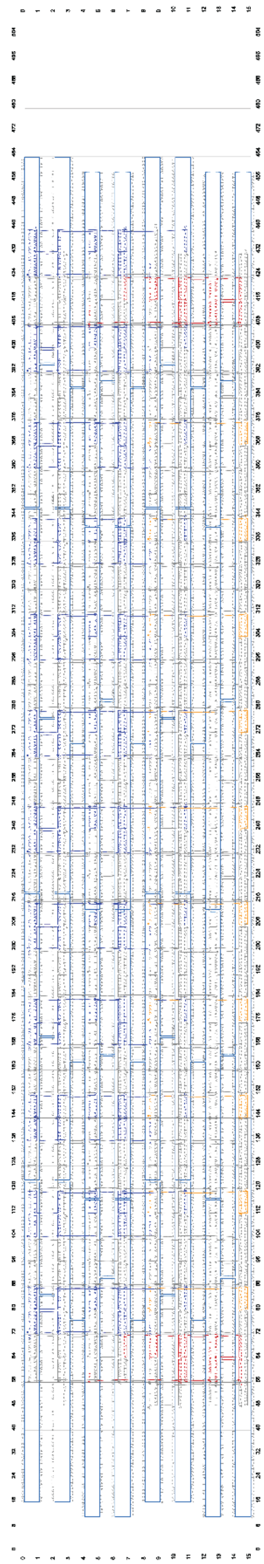

Figure S13. Schematic of the 16HB origami generated by caDNAno. Blue: p7560 scaffold strand, Red: hairpin binding staples. Orange: particle binding staples. Additional information showing full staple sequences can be found in **Table S1-3**.

Table S1.
Oligonucleotide ID and sequences used in this work.

Strand ID	DNA Sequences (5' to 3')
particle-linker (sequence b*)	GCA GTG TGT GAG TGG TTT CAG TTT /3AzideN/
hairpin	CTG AAA CCA CTC ACA CAC TGC /iUniAmM/ GTA TAA ATG TTT TTT TCA TTT ATA C AGC GCC ACG TAG CCC AGC
no-stem-loop	CTG AAA CCA CTC ACA CAC TGC/iUniAmM/AGC GCC ACG TAG CCC AGC
17-mer	GAA AAA AAC ATT TAT AC
anchor 1 (sequence a*)	TTTCAGGGCCACCCTCCGATTGGCGAATCAAGGTCACCAA-TT-GCTGGGCTACGTGGCGCT
anchor 2 (sequence a*)	CGGAACCTGTTTTAACGCCAGAATCCGGAAACTTTGCCTT-TT-GCTGGGCTACGTGGCGCT
anchor 3 (sequence a*)	AGGTCAGAAGAACCGCTTCATAATCAAAATCA-TT-GCTGGGCTACGTGGCGCT
anchor 4 (sequence a*)	GCGTTATAGCACCCAGCCGGTATTCGTCAAAAGACGGGAG-TT-GCTGGGCTACGTGGCGCT
anchor 5 (sequence a*)	AGCATGTAAATAATCGTACCGCGCGCGCATTAATGAAAAT-TT-GCTGGGCTACGTGGCGCT
anchor 6 (sequence a*)	AGGCTTATCTACAATTTCTTACCAACGCTAAC-TT-GCTGGGCTACGTGGCGCT
crosslink 1 (sequence b)	CTGAAACCACTCACACACTGC-TT-ACATAAAAAATAGCTAAACAGTAC
crosslink 2 (sequence b)	CTGAAACCACTCACACACTGC-TT-AACGTTATAAGTAAGCTTTTCAGG
crosslink 3 (sequence b)	CTGAAACCACTCACACACTGC-TT-AATTCGACAGGAAACCCAGAAGAT
crosslink 4 (sequence b)	CTGAAACCACTCACACACTGC-TT-TATGATACACCCAAAAGTGCCTAA
crosslink 5 (sequence b)	CTGAAACCACTCACACACTGC-TT-CTAATCTAATTACGCAACGAGCCG
crosslink 6 (sequence b)	CTGAAACCACTCACACACTGC-TT-TATGACAACATACATAATCTGCCA
crosslink 7 (sequence b)	CTGAAACCACTCACACACTGC-TT-CTTAAGTGGCAAAGACATATCGCG
crosslink 8 (sequence b)	CTGAAACCACTCACACACTGC-TT-GTCAGGACACAATCAAAAAAGATT
crosslink 9 (sequence b)	CTGAAACCACTCACACACTGC-TT-TATGCGATCGCCAAAGTATTATAG
crosslink 10 (sequence b)	CTGAAACCACTCACACACTGC-TT-TTAATTTCTGAGGGAGTGTGTCGA

Table S2.
Origami scaffold sequence (p7560)

AGCTTGGCACTGGCCGTCGTTTTACAACGTCGTGACTGGGAAAACCCTGGCGTTACCCAA
CTTAATCGCCTTGCAGCACATCCCCCTTTCGCCAGCTGGCGTAATAGCGAAGAGGCCCGC
ACCGATCGCCCTTCCCAACAGTTGCGCAGCCTGAATGGCGAATGGCGCTTTGCCTGGTTTC
CGGCACCAGAAGCGGTGCCGGAAAGCTGGCTGGAGTGCGATCTTCCTGAGGCCGATACTG
TCGTCGTCCCCTCAAACTGGCAGATGCACGGTTACGATGCGCCCATCTACACCAACGTGA
CCTATCCCATTACGGTCAATCCGCCGTTTGTTCCCACGGAGAATCCGACGGGTTGTTACTC
GCTCACATTTAATGTTGATGAAAGCTGGCTACAGGAAGGCCAGACGCGAATTATTTTTGA
TGGCGTTCCTATTGGTTAAAAAATGAGCTGATTTAACAAAAATTTAATGCGAATTTTAACA
AAATATTAACGTTTACAATTTAAATATTTGCTTATACAATCTTCCTGTTTTTGGGGCTTTTC
TGATTATCAACCGGGGTACATATGATTGACATGCTAGTTTTACGATTACCGTTCATCGATT
CTCTTGTTTGCTCCAGACTCTCAGGCAATGACCTGATAGCCTTTGTAGATCTCTCAAAAAT
AGCTACCCTCTCCGGCATTAATTTATCAGCTAGAACGGTTGAATATCATATTGATGGTGAT
TTGACTGTCTCCGGCCTTTCTCACCCTTTTGAATCTTTACCTACACATTACTCAGGCATTGC
ATTTAAAATATATGAGGGTTCTAAAAATTTTTATCCTTGCGTTGAAATAAAGGCTTCTCCC
GCAAAAGTATTACAGGGTCATAATGTTTTTGGTACAACCGATTTAGCTTTATGCTCTGAGG
CTTTATTGCTTAATTTTGCTAATTCTTTGCCTTGCCTGTATGATTTATTGGATGTTAATGCTA
CTACTATTAGTAGAATTGATGCCACCTTTTCAGCTCGCGCCCCAAATGAAAATATAGCTAA
ACAGGTTATTGACCATTTGCGAAATGTATCTAATGGTCAAACTAAATCTACTCGTTCGCAG
AATTGGGAATCAACTGTTATATGGAATGAAACTTCCAGACACCGTACTTTAGTTGCATATT
TAAAACATGTTGAGCTACAGCATTATATTCAGCAATTAAGCTCTAAGCCATCCGCAAAAA
TGACCTCTTATCAAAAGGAGCAATTAAAGGTACTCTCTAATCCTGACCTGTTGGAGTTTGC
TTCCGGTCTGGTTCGCTTTGAAGCTCGAATTAAAACGCGATATTTGAAGTCTTTCGGGCTT
CCTCTTAATCTTTTTGATGCAATCCGCTTTGCTTCTGACTATAATAGTCAGGGTAAAGACCT
GATTTTTGATTTATGGTCATTCTCGTTTTCTGAACTGTTTAAAGCATTTGAGGGGGATTCAA
TGAATATTTATGACGATTCCGCAGTATTGGACGCTATCCAGTCTAAACATTTTACTATTAC
CCCCTCTGGCAAAACTTCTTTTGCAAAAGCCTCTCGCTATTTTGGTTTTTATCGTCGTCTGG
TAAACGAGGGTTATGATAGTGTTGCTCTTACTATGCCTCGTAATTCCTTTTGGCGTTATGTA
TCTGCATTAGTTGAATGTGGTATTCCTAAATCTCAACTGATGAATCTTTCTACCTGTAATA
ATGTTGTTCCGTTAGTTCGTTTTATTAACGTAGATTTTTCTTCCCAACGTCCTGACTGGTAT
AATGAGCCAGTTCTTAAAATCGCATAAGGTAATTCACAATGATTAAAGTTGAAATTAAAC
CATCTCAAGCCCAATTTACTACTCGTTCTGGTGTTTCTCGTCAGGGCAAGCCTTATTCACTG
AATGAGCAGCTTTGTTACGTTGATTTGGGTAATGAATATCCGGTTCTTGTCAAGATTACTC
TTGATGAAGGTCAGCCAGCCTATGCGCCTGGTCTGTACACCGTTCATCTGTCCTCTTTCAA
AGTTGGTCAGTTCGGTTCCCTTATGATTGACCGTCTGCGCCTCGTTCCGGCTAAGTAACAT
GGAGCAGGTCGCGGATTTCGACACAATTTATCAGGCGATGATACAAATCTCCGTTGTACTT
TGTTTCGCGCTTGGTATAATCGCTGGGGGTCAAAGATGAGTGTTTTAGTGTATTCTTTTGC
CTCTTTCGTTTTAGGTTGGTGCCTTCGTAGTGGCATTACGTATTTTACCCGTTTAATGGAAA
CTTCCTCATGAAAAAGTCTTTAGTCCTCAAAGCCTCTGTAGCCGTTGCTACCCTCGTTCCG
ATGCTGTCTTTCGCTGCTGAGGGTGACGATCCCGCAAAAGCGGCCTTTAACTCCCTGCAAG
CCTCAGCGACCGAATATATCGGTTATGCGTGGGCGATGGTTGTTGTCATTGTCGGCGCAAC
TATCGGTATCAAGCTGTTTAAGAAATTCACCTCGAAAGCAAGCTGATAAACCGATACAAT
TAAAGGCTCCTTTTGGAGCCTTTTTTTTGGAGATTTTCAACGTGAAAAAATTATTATTCGC
AATTCCTTTAGTTGTTCCTTTCTATTCTCACTCCGCTGAAACTGTTGAAAGTTGTTTAGCAA
AATCCCATACAGAAAATTCATTTACTAACGTCTGGAAAGACGACAAAACTTTAGATCGTT
ACGCTAACTATGAGGGCTGTCTGTGGAATGCTACAGGCGTTGTAGTTTGTACTGGTGACG
AAACTCAGTGTTACGGTACATGGGTTCCTATTGGGCTTGCTATCCCTGAAAATGAGGGTGG
TGGCTCTGAGGGTGGCGGTTCTGAGGGTGGCGGTTCTGAGGGTGGCGGTACTAAACCTCC

TGAGTACGGTGATACACCTATTCCGGGCTATACTTATATCAACCCTCTCGACGGCACTTAT
CCGCCTGGTACTGAGCAAAACCCCGCTAATCCTAATCCTTCTCTTGAGGAGTCTCAGCCTC
TTAATACTTTCATGTTTCAGAATAATAGGTTCCGAAATAGGCAGGGGGCATTAACTGTTTA
TACGGGCACTGTTACTCAAGGCACTGACCCCGTTAAAACTTATTACCAGTACACTCCTGTA
TCATCAAAAGCCATGTATGACGCTTACTGGAACGGTAAATTCAGAGACTGCGCTTTCCATT
CTGGCTTTAATGAGGATTTATTTGTTTGTGAATATCAAGGCCAATCGTCTGACCTGCCTCA
ACCTCCTGTCAATGCTGGCGGCGGCTCTGGTGGTGGTTCTGGTGGCGGCTCTGAGGGTGGT
GGCTCTGAGGGTGGCGGTTCTGAGGGTGGCGGCTCTGAGGGAGGCGGTTCCGGTGGTGGC
TCTGGTTCCGGTGATTTTGATTATGAAAAGATGGCAAACGCTAATAAGGGGGCTATGACC
GAAAATGCCGATGAAAACGCGCTACAGTCTGACGCTAAAGGCAAACTTGATTCTGTCGCT
ACTGATTACGGTGCTGCTATCGATGGTTTCATTGGTGACGTTTCCGGCCTTGCTAATGGTA
ATGGTGCTACTGGTGATTTTGCTGGCTCTAATTCCCAAATGGCTCAAGTCGGTGACGGTGA
TAATTCACCTTTAATGAATAATTTCCGTCAATATTTACCTTCCCTCCCTCAATCGGTTGAAT
GTCGCCCTTTTGTCTTTGGCGCTGGTAAACCATATGAATTTTCTATTGATTGTGACAAAAT
AAACTTATTCCGTGGTGTCTTTGCGTTTCTTTTATATGTTGCCACCTTTATGTATGTATTTTC
TACGTTTGCTAACATACTGCGTAATAAGGAGTCTTAATCATGCCAGTTCTTTTGGGTATTC
CGTTATTATTGCGTTTCCTCGGTTTCCTTCTGGTAACTTTGTTCGGCTATCTGCTTACTTTTC
TTAAAAAGGGCTTCGGTAAGATAGCTATTGCTATTTCATTGTTTCTTGCTCTTATTATTGGG
CTTAACTCAATTCTTGTGGGTTATCTCTCTGATATTAGCGCTCAATTACCCTCTGACTTTGT
TCAGGGTGTTCAGTTAATTCTCCCGTCTAATGCGCTTCCCTGTTTTTATGTTATTCTCTCTGT
AAAGGCTGCTATTTTCATTTTTGACGTTAAACAAAAAATCGTTTCTTATTTGGATTGGGAT
AAATAATATGGCTGTTTATTTTGTAACTGGCAAATTAGGCTCTGGAAAGACGCTCGTTAGC
GTTGGTAAGATTCAGGATAAAATTGTAGCTGGGTGCAAAATAGCAACTAATCTTGATTTA
AGGCTTCAAAACCTCCCGCAAGTCGGGAGGTTCGCTAAAACGCCTCGCGTTCTTAGAATA
CCGGATAAGCCTTCTATATCTGATTTGCTTGCTATTGGGCGCGGTAATGATTCCTACGATG
AAAATAAAAACGGCTTGCTTGTTCTCGATGAGTGCGGTACTTGGTTTAATACCCGTTCTTG
GAATGATAAGGAAAGACAGCCGATTATTGATTGGTTTCTACATGCTCGTAAATTAGGATG
GGATATTATTTTTCTTGTTCAGGACTTATCTATTGTTGATAAACAGGCGCGTTCTGCATTAG
CTGAACATGTTGTTTATTGTCGTCGTCTGGACAGAATTACTTTACCTTTTGTCGGTACTTTA
TATTCTCTTATTACTGGCTCGAAAATGCCTCTGCCTAAATTACATGTTGGCGTTGTTAAATA
TGGCGATTCTCAATTAAGCCCTACTGTTGAGCGTTGGCTTTATACTGGTAAGAATTTGTAT
AACGCATATGATACTAAACAGGCTTTTTCTAGTAATTATGATTCCGGTGTTTATTCTTATTT
AACGCCTTATTTATCACACGGTCGGTATTTCAAACCATTAAATTTAGGTCAGAAGATGAAA
TTAACTAAAATATATTTGAAAAAGTTTTCTCGCGTTCTTTGTCTTGCGATTGGATTTGCATC
AGCATTTACATATAGTTATATAACCCAACCTAAGCCGGAGGTTAAAAAGGTAGTCTCTCA
GACCTATGATTTTGATAAATTCACTATTGACTCTTCTCAGCGTCTTAATCTAAGCTATCGCT
ATGTTTTCAAGGATTCTAAGGGAAAATTAATTAATAGCGACGATTTACAGAAGCAAGGTT
ATTCACTCACATATATTGATTTATGTACTGTTTCCATTAAAAAAGGTAATTCAAATGAAAT
TGTTAAATGTAATTAATTTTGTTTTCTTGATGTTTGTTTCATCATCTTCTTTTGCTCAGGTAA
TTGAAATGAATAATTCGCCTCTGCGCGATTTTGTAACTTGGTATTCAAAGCAATCAGGCGA
ATCCGTTATTGTTTCTCCCGATGTAAAAGGTACTGTTACTGTATATTCATCTGACGTTAAAC
CTGAAAATCTACGCAATTTCTTTATTTCTGTTTTACGTGCAAATAATTTTGATATGGTAGGT
TCTAACCCTTCCATTATTCAGAAGTATAATCCAAACAATCAGGATTATATTGATGAATTGC
CATCATCTGATAATCAGGAATATGATGATAATTCCGCTCCTTCTGGTGGTTTCTTTGTTCCG
CAAAATGATAATGTTACTCAAACTTTTAAAATTAATAACGTTCGGGCAAAGGATTTAATA
CGAGTTGTCGAATTGTTTGTAAAGTCTAATACTTCTAAATCCTCAAATGTATTATCTATTG
ACGGCTCTAATCTATTAGTTGTTAGTGCTCCTAAAGATATTTTAGATAACCTTCCTCAATTC
CTTTCAACTGTTGATTTGCCAACTGACCAGATATTGATTGAGGGTTTGATATTTGAGGTTC
AGCAAGGTGATGCTTTAGATTTTTCATTTGCTGCTGGCTCTCAGCGTGGCACTGTTGCAGG
CGGTGTTAATACTGACCGCCTCACCTCTGTTTTATCTTCTGCTGGTGGTTCGTTCGGTATTT
TTAATGGCGATGTTTTAGGGCTATCAGTTCGCGCATTAAAGACTAATAGCCATTCAAAAAT

ATTGTCTGTGCCACGTATTCTTACGCTTTCAGGTCAGAAGGGTTCTATCTCTGTTGGCCAG
AATGTCCCTTTTATTACTGGTCGTGTGACTGGTGAATCTGCCAATGTAAATAATCCATTTC
AGACGATTGAGCGTCAAAATGTAGGTATTTCCATGAGCGTTTTTCCTGTTGCAATGGCTGG
CGGTAATATTGTTCTGGATATTACCAGCAAGGCCGATAGTTTGAGTTCTTCTACTCAGGCA
AGTGATGTTATTACTAATCAAAGAAGTATTGCTACAACGGTTAATTTGCGTGATGGACAG
ACTCTTTTACTCGGTGGCCTCACTGATTATAAAAACACTTCTCAGGATTCTGGCGTACCGT
TCCTGTCTAAAATCCCTTTAATCGGCCTCCTGTTTAGCTCCCGCTCTGATTCTAACGAGGA
AAGCACGTTATACGTGCTCGTCAAAGCAACCATAGTACGCGCCCTGTAGCGGCGCATTAA
GCGCGGCGGGTGTGGTGGTTACGCGCAGCGTGACCGCTACACTTGCCAGCGCCCTAGCGC
CCGCTCCTTTCGCTTTCTTCCCTTCCTTTCTCGCCACGTTCGCCGGCTTTCCCCGTCAAGCTC
TAAATCGGGGGCTCCCTTTAGGGTTCCGATTTAGTGCTTTACGGCACCTCGACCCCAAAAA
ACTTGATTTGGGTGATGGTTCACGTAGTGGGCCATCGCCCTGATAGACGGTTTTTCGCCCT
TTGACGTTGGAGTCCACGTTCTTTAATAGTGGACTCTTGTTCCAAACTGGAACAACACTCA
ACCCTATCTCGGGCTATTCTTTTGATTTATAAGGGATTTTGCCGATTTCGGAACCACCATC
AAACAGGATTTTCGCCTGCTGGGGCAAACCAGCGTGGACCGCTTGCTGCAACTCTCTCAG
GGCCAGGCGGTGAAGGGCAATCAGCTGTTGCCCGTCTCACTGGTGAAAAGAAAAACCACC
CTGGCGCCCAATACGCAAACCGCCTCTCCCCGCGCGTTGGCCGATTCATTAATGCAGCTGG
CACGACAGGTTTCCCGACTGGAAAGCGGGCAGTGAGCGCAACGCAATTAATGTGAGTTAG
CTCACTCATTAGGCACCCCAGGCTTTACACTTTATGCTTCCGGCTCGTATGTTGTGTGGAA
TTGTGAGCGGATAACAATTTCACACAGGAAACAGCTATGACCATGATTACGAATTCGAGC
TCGGTACCCGGGGATCCTCCGTCTTTATCGAGGTAACAAGCACCACGTAGCTTAAGCCCTG
TTTACTCATTACACCAACCAGGAGGTCAGAGTTCGGAGAAATGATTTATGTGAAATGCGT
CAGCCGATTCAAGGCCCCTATATTCGTGCCCACCGACGAGTTGCTTACAGATGGCAGGGC
CGCACTGTCGGTATCATAGAGTCACTCCAGGGCGAGCGTAAATAGATTAGAAGCGGGGTT
ATTTTGGCGGGACATTGTCATAAGGTTGACAATTCAGCACTAAGGACACTTAAGTCGTGC
GCATGAATTCACAACCACTTAGAAGAACATCCACCCTGGCTTCTCCTGAGAA

Table S3.
Origami staples. Hairpin binding sites are labeled in red, crosslinker sites are highlighted in gray.
To make the Δ32 structure, staples that are underlined were withheld from assembly solution.

Start	End	Sequence	Length
0[71]	5[71]	AATAGTGACAAGACAAAATTCTGTTCGAGCCA	32
0[103]	5[103]	CGATAGCTATCGTCGCACAAAATCGAATTATT	32
0[135]	5[135]	TTTGATTACACTTGCCGAATGGCTTGGCCAAC	32
0[167]	5[167]	ATCACGCAGCCTTGCTGGTTAAGAAAGCGTTG	32
0[199]	5[199]	AACCGTCTAGAGTCCAATTAATGATCTTTTCA	32
0[231]	5[231]	ATATGATACTAGCTGAGAGTAACAGCATTAAA	32
0[263]	5[263]	GAGAAAGGTATTTTTGGTAGCCAGTAACCAAT	32
0[295]	5[295]	TGAGTAATTCGGTTGTATTGCTGAGTAGCTCA	32
0[327]	5[327]	TTAGAACCTACTTTTGAGAGGTCAGTACGGTG	32
0[359]	5[359]	CCGATAGTATGACAACCTCATCTTAAATACGT	32
0[391]	5[391]	CTTTCGAGATATTCGGAGGCGAAATAAAAGTT	32
0[423]	5[423]	GGAGCCTTAGCGGAGTTGCTCAGTTGTATCAC	32
1[56]	7[63]	TCCAATCGATTTATCAAATTTACG	24
1[88]	7[95]	TTCTGTAATAGATTAAGAAACAAT	24
1[120]	7[127]	CTTAACATGTAATAGACGCGAACT	24
1[152]	7[159]	AACTATCGAATTAACCAAAATACC	24
1[184]	7[191]	TTGGAACAATCACCGACACTGCCC	24
1[216]	7[223]	ACTCCGTTTTCAACCACCGTGGGA	24
1[248]	7[255]	AGGGTAGCCCGGAGACGGATAGGT	24
1[280]	7[287]	AAGCTAAAGTGTAGGTTCAAAGCG	24
1[312]	7[319]	CCCTGTAACTCATATACAGGTCAG	24
1[344]	7[351]	TTCCGACATGCGCAACTATACCAA	24
1[376]	7[383]	TAACCGATGTGAATTTTTTGTATC	24
1[408]	7[415]	ACAGTTTCTAATTGTAGCCTATTT	24
2[71]	4[64]	TATTTTAGTAGAAAAATATCATAT	24
2[103]	4[96]	ATATGTGATTTCATTTATGATGAA	24
2[135]	4[128]	CAGGAAAAAAATACCTGTCACACG	24
2[167]	4[160]	ATCCAGAAAATGGTCCCAAGCGGA	24
2[199]	4[192]	ATCAAAAGAAATCCTGCCCTTCAC	24
2[231]	4[224]	GATGAACGAACTAGCAATTGTAAA	24
2[263]	4[256]	TTGCCTGAATAATCAGAAAACAGG	24
2[295]	4[288]	AGCAATAACTATATTTGTTTGACC	24
2[327]	4[320]	CATACAGGGTGGCATCTTGATTCC	24
2[359]	4[352]	GGATCGTCGCGAAAGATTTCATGA	24
2[391]	4[384]	AGGCTTGCGGCCATGTGAACCTAC	24
2[423]	4[416]	GTAAATGAAGTACAAAACCCTCAT	24
3[48]	5[63]	CCGGAATCATAATTACTTAATTTCAGGCATTT	32
3[80]	5[95]	TAATTACATTTAACAAGTGAATAAAGGAGGC	32
3[112]	5[127]	TTTTTTAATGGCATGGACGCTAAAGGACATTC	32
3[144]	5[159]	ACGCTCAATCGTCTGACAATATTATGACCTGA	32

3[176]	5[191]	TTGCCCCAGCAGGCGAAATAGCCCGTGGTTTT	32
3[208]	5[223]	TGGTTCCGAAACGTAAGTAATTCGTAAAATTC	32
3[240]	5[255]	ATATGTACCCCGGTTGGAGTCTGGTCATTTTT	32
3[272]	5[287]	TCAATAACCTGTTTAGAGCCTCAGATAATGCT	32
3[304]	5[319]	GGCGCGAGCTGAAAAGCAAGGCAACAACTAAA	32
3[336]	5[351]	TAATAGTAGTACAGCAACCCTGCAAACGGGTA	32
3[368]	5[383]	GAACGAGGGTAGCAACAGGGAGTTCACCAACC	32
3[400]	5[415]	ACTGAGTTTCGTCACCATTTTCTGGGAATAGG	32
4[63]	14[56]	GCGTTATAGCACCCAGCCGGTATTCGTCAAAAGACGGGAG	40
4[95]	14[88]	ACAAACATAATTCATCTACCATATAGACATTAAGTAAATA	40
4[127]	14[120]	ACCAGTAAATAATCAACCTCACTTATTAGAGCTTTGCCCG	40
4[159]	14[152]	TTATTTACAGTTGAAAAGCATCACATTTAGAATTACAAAC	40
4[191]	14[184]	CGCCTGGCCAGGGCTTCTCGAATTCTCGTCGGAGTGACTC	40
4[223]	14[216]	CGTTAATAGATTGCGGATCGGAAACAGTGCCACCCCGCTT	40
4[255]	14[248]	AAGATTGTGCGAAAGGCCATTCAGGGATGTTCGTCAACCT	40
4[287]	14[280]	ATTAGATACCTCGTTTTATTCATTGCATAATATACGTCGA	40
4[319]	14[312]	CAATTCTGTAGCGAGAGATAGCGTTTACAGGTTTATACCA	40
4[351]	14[344]	GGAAGTTTAGATAGGCGCGCAGGGATAAGGCTAATTACCT	40
4[383]	14[376]	AGAGGCTTCTTGACAAGAAAGAGGGAGTAGTAGAGATGGT	40
4[415]	14[408]	TTTCAGGGCCACCCTCCGATTGGCGAATCAAGGTCACCAA	40
6[63]	15[63]	CCAGACGAGGAATCATGCTGTCTTAAGAGCAA	32
6[87]	0[72]	CGACAAAACATCGGGAGACGCTGAGAAGAGTC	32
6[95]	15[95]	GCGCATACTATTTGCATATACAGTTCTTACCG	32
6[119]	0[104]	TTATGAATTGCTTATGATCCTTGAAAACATAG	32
6[127]	15[127]	ATTAGTCTCGTGTATTGGTCAAGAAGATAGCC	32
6[151]	0[136]	CACAGACACGCCATTAGTTGTAGCAATACTTC	32
6[159]	15[159]	ATACGTGGCTGAGAGCACCACCAGGAGGAAAC	32
6[183]	0[168]	ACGCGCGGGTTGCGCTGTAAAAGAGTCTGTCC	32
6[191]	15[191]	ATCGGCCAGTGTGAAAAGCCTGGGGAACTGGC	32
6[215]	0[200]	GATTCGTGACCTGTCTACGTCAAAGGGCGAAA	32
6[223]	15[223]	ACCCGTCGCAAATCGGACAGTCATGTATGTTA	32
6[247]	0[232]	AACATTAACCGTAATGAGTCAAATCACCATCA	32
6[255]	15[255]	CTTTCATCAGCTTTCCAACCGTGCAAGGTGGC	32
6[279]	0[264]	CGCGTCTGTTCGAGCTAAAGATTCAAAAGGGT	32
6[287]	15[287]	ATATAATTCCCTCAAAGACTTCAAACCACGGA	32
6[311]	0[296]	GATGGCTTAACTCCAATTTTAAATGCAATGCC	32
6[319]	15[319]	TTTTTGCGGAATGACCTTGCATCATAGAAAAT	32
6[343]	0[328]	AGCGCTCCTAATTGATGCAAGGATAAAAATTT	32
6[351]	15[351]	TGACCCCCCCTTACTTCATGTGACACAAAAGG	32
6[375]	0[360]	AGAATACAAACGGAGACTTAAACAGCTTGATA	32
6[383]	15[383]	GAGGCAAAAATCATAATGATAAATGGAAGGTA	32
6[407]	0[392]	GATAAGTGTGCCCCCTTCGGTTTATCAGCTTG	32
6[415]	15[415]	ACCAGGCGTCATTAAAGGGGTCAGAAGGTGAA	32

6[439]	0[424]	AGGATTAGGAAACATGAAAAAAGGCTCCAAAA	32
7[64]	13[71]	AGCATGTAAATAATCGTACCGCGCGCATTAATGAAAAT	40
7[96]	13[103]	AACGGATTCAGATGAACGTAAAACAAAGTTTGTCATTTTG	40
7[128]	13[135]	GATAGCCCGGTGAGGCAACACCGCTTAAATCCCGTCAATA	40
7[160]	13[167]	GAATCACACTAACCGACAGCAGCACGGAGACTGTATTCCC	40
7[192]	13[199]	GCTTTCCAAAGTGTAATTGTTATCCGCCCTGGTGGGCACG	40
7[224]	13[231]	ACAAACGGGGACGACGCCTCAGGACAAAATAAAGCTTTCT	40
7[256]	13[263]	CACGTTGGCGCATCGTGGCACCGCGCTGAATTTTCTAAGT	40
7[288]	13[295]	AACCAGACGCCCGAAATGCTTTAAGAAAAATCAAACGAAC	40
7[320]	13[327]	GATTAGAGAAAGCGGAATAAATCACTGGCTCAAGAAAGAT	40
7[352]	13[359]	GCGCGAAAACCTGCTCAGCCGGAATCATTGTGTGCCCTGA	40
7[384]	13[391]	ATCTATAAGCCCGGCCGGGAACCGAGCGGCTTAATTGACC	40
7[416]	13[423]	CGGAACCTGTTTTAACGCCAGAATCCGGAAACTTTGCCTT	40
8[79]	2[72]	CTTCAATCGAAACTTAGGTAAAGTAGAACGCGTTCAAATA	40
8[111]	2[104]	TTTAACGTCGCCTGATACCAAGTTTATTAATTAAATCAAT	40
8[143]	2[136]	AAAACAGATAAAACATATATTTTTTGAGTAGACATTGCAA	40
8[175]	2[168]	TGAGTGAGTTAATTGCGGAGAGGCGGTGTGTTGTTGAAAT	40
8[207]	2[200]	GAAGCATAGTCGGGAACCAGCTGCCTATTAAACCTTATAA	40
8[239]	2[232]	GTTTGAGGCGGATTGAATGTGAGCTAAATTAAAGAGAATC	40
8[271]	2[264]	TTTATGGGTGTAGTAAGCCTTCCTAGAGATCTTCAGGTCA	40
8[303]	2[296]	AAGAGGAACGGAAGCAAGAGCTTAACCAAAAACAAAATTA	40
8[335]	2[328]	TCAGAAGCAGTACCTTTTTTGATACGGGAGAACAATAAAT	40
8[367]	2[360]	AATCCGCGCAAAGTACCTAAAACAAACCATCGCTTTTGCG	40
8[399]	2[392]	GTAACAGTACAGTTAACCGTCGAGTCGTAAACTTTGCCTG	40
8[431]	2[424]	GGTAATAAATTATTCTCGGGGTTTGAGAATAGAGACGTTA	40
10[71]	12[56]	AGGCTTATCTACAATTTCTTACCAACGCTAAC	32
10[103]	12[88]	TTAGAACCAATATAATCGGAATTATCATCATA	32
10[135]	12[120]	TATCAAACTATCTGGTTAGGAGCACTAACAAC	32
10[167]	12[152]	AAATCTAAGGACTGGTACCTCATTGAGGAAGG	32
10[199]	12[184]	GTACCGAGAAGCTACGGCATTTCACATAAATC	32
10[231]	12[216]	GAAGGGCGGCCTCTTCCACGACGTTGTAAAAC	32
10[263]	12[248]	GCCATTCGGGGATGTGATTAAGTTGGGTAACG	32
10[295]	12[280]	GTCATAAAACCAGACGGGAATTACGAGGCATA	32
10[327]	12[312]	TTAGACTGGGCTTTTGCATTCAACTAATGCAG	32
10[359]	12[344]	CAGACCAGTGGCTGACAACAAAGCTGCTCATT	32
10[391]	12[376]	CCAACTTTGAAGAACCCACCGCCGGATATTCA	32
10[423]	12[408]	AGGTCAGAAGAACCGCTTCATAATCAAAATCA	32
10[79]	3[79]	GATATAGAGTAATAAGCAATTTAGGCCTGAAT	32
10[143]	3[143]	ACCTCAAAAGAGATAGATTCACCAACATTTTG	32
10[111]	3[111]	TGGAAGGGCATTTCAAAAAAGAAGGAATTACC	32
10[175]	3[175]	TGGTCGAACGTATTGGAGTTGCAGACGCTGGT	32
10[207]	3[207]	ATCCCCGGCCAGTGAGGCTGATTGTTTGATGG	32
10[239]	3[239]	ACTGTTGGTTTTTGTTATATTTAATGTCAATC	32

10[271]	3[271]	GGCAAAGCAGGAACGCAAACCCCAAAAAGTGG	32
10[303]	3[303]	GCGGAATCACATGTTTTAGATTTATCATTTGG	32
10[335]	3[335]	TAAAATGTTCTGGAAGTATAACAGAATTCTAC	32
10[367]	3[367]	ACGGTGTAAATGCCACAAAGACTTCAGCATCG	32
10[399]	3[399]	TCACATGAGATATAAGCCCAATAGACCGTAAC	32
10[431]	3[431]	GTTGAGGCCGTACTCAGAGCCACCCTACAACG	32
11[80]	1[87]	ATGATGGCCAAGAAAAAGAATATACCTACTTTAGAAATGC	40
11[112]	1[119]	TTTGGATTTAATGAGCTTACCAAGCAGTACATAATTTTCC	40
11[144]	1[151]	AAATCAACATTGGCAGAACCCTTCCCGCCAGCAGAACTCA	40
11[176]	1[183]	TGAGTAAACCTGAGAGGCGCCAGGGAGATAGGGTTCCAGT	40
11[208]	1[215]	GTTACCTCTTTCAACAACGGGTGTGCAAAATCGAACGTGG	40
11[240]	1[247]	GCCAGCTGATAAGCAAAAATCAGCAGCAAACATGCCGGAG	40
11[272]	1[279]	ATCATAACCATTTCGCCATCAAAAAGCGGCTAACAAAATA	40
11[304]	1[311]	AACCAAAACGAACGAGTAAATATGAGAATTAGCATTATGA	40
11[336]	1[343]	GTTTTGCCCCATTCCATTTCATTATTAACATCGCCTTTAT	40
11[368]	1[375]	AGAGTAATTGAGGACTTACGAAGGAAAGGCCGCCCACGCA	40
11[400]	1[407]	CAGAGCCGATAGCAAGTATAGCCCTATGGGATAACTTTCA	40
11[432]	1[439]	GAGCCACCCACCCTCAGGAGGTTTGTCTTTCCAAAGGAAC	40
12[55]	9[55]	GAGCGTCTTTGTTTAACTAAGAACTCATCGTA	32
12[87]	9[87]	TTCCTGATTTACAGAGCAAAATCAAAGCAAAT	32
12[119]	9[119]	TAACCACCAGAAATAGCTGAATAAAGAAATTG	32
12[151]	9[151]	TTATCTAAATTTGAGGCTTGCTGAGTGCCACG	32
12[183]	9[183]	ATTTCTCCGTAAGCAACGTAATCATGTTTCCT	32
12[215]	9[215]	GACTGAATGGCCTGGCGACGGAGGATTCCACA	32
12[247]	9[247]	CCAGGGTTGCCAGGGTGCTGCGCACTCCAGCC	32
12[279]	9[279]	GTAAGAGCATTCATGCGAAAACCACCGGATCC	32
12[311]	9[311]	ATACATAACAACATTACCAATACTGAAAACGA	32
12[343]	9[343]	CAGTTTAGTGAGATGAGGTAATAGGTCTTTAC	32
12[375]	9[375]	TTACCCAAACCAGAACACAGATGAAGACGGTC	32
12[407]	9[407]	CCGGAACCTAGCGACACTTGATATATAAATCC	32
13[72]	11[79]	AGCAGCCTTATCTGAATTATCCAG	24
13[104]	11[111]	CGGAACAAAGAAGGAGCCTGATTG	24
13[136]	11[143]	GATAATACAATATCTTCAGTTGGC	24
13[168]	11[175]	TGCCATCTGAACTCTGTGGTGTAA	24
13[200]	11[207]	AATATAGGCGGCTGACTGGTGCTT	24
13[232]	11[239]	CAGGAGAATTCCCAGTGCTATTAC	24
13[264]	11[271]	GGTTGTGAAACAGGCGCTGCAACT	24
13[296]	11[303]	TAACGGAACGCCAAAAACGATAAA	24
13[328]	11[335]	TCATCAGTGAATACCACAAAAGAA	24
13[360]	11[367]	CGAGAAACATCAACGTCTTCATCA	24
13[392]	11[399]	GTAATCAGAGAGCCACGCCTCCCT	24
13[424]	11[431]	TAGCGTCAGCCATCTTCACCCTCA	24
14[55]	8[47]	AATTAACTCCAATAATTCCTTATCA	25

14[87]	8[80]	ACATAAAAAATAGCTAAACAGTAC	24
14[119]	8[112]	AACGTTATAAGTAAGCTTTTCAGG	24
14[151]	8[144]	AATTCGACAGGAAACCCAGAAGAT	24
14[183]	8[176]	TATGATACACCCAAAAGTGCCTAA	24
14[215]	8[208]	CTAATCTAATTACGCAACGAGCCG	24
14[247]	8[240]	TATGACAACATACATAATCTGCCA	24
14[279]	8[272]	CTTAAGTGGCAAAGACATATCGCG	24
14[311]	8[304]	GTCAGGACACAATCAAAAAAGATT	24
14[343]	8[336]	TATGCGATCGCCAAAGTATTATAG	24
14[375]	8[368]	TTAATTTCTGAGGGAGTGTGTCGA	24
14[407]	8[400]	TGAAACCAATTCATTATGCCTTGA	24
15[64]	9[79]	GAAACAATGAAATAGCACAGGGAACCAATAGC	32
15[96]	9[111]	AAGCCCTTTTTAAGAATAATTTTAAGAAATAA	32
15[128]	9[143]	GAACAAAGTTACCAGAAACTCGTACTGCAACA	32
15[160]	9[175]	GCAATAATAACGGAATCGACAGTGAATATAGC	32
15[192]	9[207]	ATGATTAAGACTCCTTTTTACGCTCGCTCACA	32
15[224]	9[239]	GCAAACGTAGAAAATATGTCCCGCAGATCGCA	32
15[256]	9[271]	AACATATAAAAGAAACTCCTTAGTTTCTGGTG	32
15[288]	9[303]	ATAAGTTTATTTTGTCGTTGGGAAACAGTTCA	32
15[320]	9[335]	TCATATGGTTTACCAGTTTAAGAAAAAATCAG	32
15[352]	9[367]	GCGACATTCAACCGATAACTTTAACGAGGCGC	32
15[384]	9[399]	AATATTGACGGAAATTTCGATAGCAACAACAA	32
15[416]	9[439]	TTATCACCGTCACCGATAGCAAGGGGAAAGCGCAGTCTCT	40

Table S4.
Reported volumetric phase transition dynamics of thermo-responsive polymer particles.

Reference	Year	Particle size	Characterization	Dynamics
Tanaka et al[26]	1988	234 μm - 3.1 time smaller	water exchange heating	The switching time of the temperature of the water was about 10 s, which is much shorter than the swelling or shrinking time of most of the gels.
Andrew Lyon Mostafa A. El-Sayed[27]	2001	200 nm	turbidity, laser T-jump transmittance signal	ns to μs, **0.39μs**
Asher et al[28]	2004	self-assembling crystalline colloidal arrays, 350 nm – 125 nm	T-jump. Diffraction for CCA single particle: turbidity	The shortest time ~ **900 ns** kinetics accounts for ~25% of the transmission change, while the longer time **~20μs** kinetics accounts for another ~25%. The longest **~140μs** kinetics accounts for the remaining 50% extinction increase. Individual NIPAM sphere switching occurs in the **~100 ns** time regime.
Asher et al[29]	2009	160nm-80nm	T-jump and UV resonance Raman (UVRR) spectroscopy	Mono-exponential collapse with **τ ~ 360 ± 85 ns**
Asher et al[30]	2018	404 nm – 143 nm	visible non-resonance Raman T-jump	The PNIPAM hydrophobic isopropyl and methylene groups dehydrate with time constants of **109 ± 64** and **104 ± 44 ns**, initiating the volume collapse of PNIPAM. The subsequent dehydration of the PNIPAM amide groups is significantly slower, as our group previously discovered (**360 ± 85 ns**)
Hu et al[31]	2009	60 μm	modeling and taking image at different timepoints	10-100 sec
Marquez et al[32]	2006	μm scale minigel	modeling and taking image at different timepoints	~ sec scale
Salaita et al[33]	2019	550 nm-350 nm	IR T-jump	**1.42 μs** (40.7%), **10.80 μs** (36.7%), **142 μs** (22.6%), 35°C to 45°C

Table S5.
Single-exponential fits of T-jump & mechanical unfolding kinetics of DNA hairpin

T jump				
		Replicate #1	Replicate #2	Replicate #3
50°C	y0	1.04206	1.04874	1.09249
	A1	-0.02576	-0.03779	-0.07818
	t1	-7.36E-05	-4.17E-05	-5.45E-05
55°C	y0	1.11706	1.10222	1.10472
	A1	-0.11873	-0.09197	-0.0954
	t1	-5.12E-05	-3.55E-05	-4.92E-05
60°C	y0	1.25246	1.18715	1.14314
	A1	-0.27482	-0.18935	-0.1496
	t1	-3.85E-05	-3.18E-05	-2.98E-05
65°C	y0	1.27531	1.27014	1.11876
	A1	-0.30072	-0.29085	-0.14145
	t1	-2.27E-05	-2.10E-05	-1.46E-05
Force jump				
		Replicate #1	Replicate #2	Replicate #3
45°C	y0	1.12115	1.08967	1.07291
	A1	-0.111	-0.06864	-0.05888
	t1	-1.66E-04	-3.70E-04	-2.06E-04
50°C	y0	1.20089	1.10659	1.08534
	A1	-0.19963	-0.09198	-0.06815
	t1	-1.08E-04	-1.66E-04	-1.64E-04
55°C	y0	1.29485	1.11821	1.05727
	A1	-0.29847	-0.11953	-0.04222
	t1	-5.41E-05	-6.72E-05	-7.27E-05
60°C	y0	1.23931	1.161	1.04781
	A1	-0.24386	-0.1643	-0.03935
	t1	-2.91E-05	-4.52E-05	-5.07E-05
65°C	y0	1.22235	1.18765	1.05924
	A1	-0.2463	-0.21118	-0.0465
	t1	-1.88E-05	-2.19E-05	-2.59E-05

Table S6.
Statistical two-way ANOVA test of angle and force of the OPFC at different configuration and temperature.

	Angle of bending			Force		
Configuration-Temperature)	Significant?	Summary	Adjusted P Value	Significant?	Summary	Adjusted P Value
L_{10nm}-40°C vs. L_{10nm}-55°C	Yes	****	<0.000000000000001	No	ns	0.999999999
L_{30nm}-40°C vs. L_{30nm}-55°C	Yes	****	<0.000000000000001	No	ns	1
L_{50nm}-40°C vs. L_{50nm}-55°C	Yes	****	<0.000000000000001	No	ns	>0.999999999999
L_{70nm}-40°C vs. L_{70nm}-55°C	Yes	****	<0.000000000000001	No	ns	0.999996866
L_{90nm}-40°C vs. L_{90nm}-55°C	Yes	****	<0.000000000000001	No	ns	0.791015348
L_{110nm}-40°C vs. L_{110nm}-55°C	Yes	****	<0.000000000000001	No	ns	0.168494339
L_{110nm}(Δ32)-40°C vs. L_{110nm}(Δ32)-55°C	Yes	****	<0.000000000000001	No	ns	0.997914188
L_{10nm}-40°C vs. L_{30nm}-40°C	No	ns	0.316370815	No	ns	>0.999999999999
L_{10nm}-40°C vs. L_{50nm}-40°C	Yes	****	<0.000000000000001	No	ns	>0.999999999999
L_{10nm}-40°C vs. L_{70nm}-40°C	Yes	****	<0.000000000000001	No	ns	>0.999999999999
L_{10nm}-40°C vs. L_{90nm}-40°C	Yes	****	<0.000000000000001	No	ns	>0.999999999999
L_{10nm}-40°C vs. L_{110nm}-40°C	Yes	****	1.40249E-06	No	ns	0.999999996
L_{10nm}-40°C vs. L_{110nm}(Δ32)-40°C	Yes	****	<0.000000000000001	No	ns	>0.999999999999
L_{10nm}-55°C vs. L_{30nm}-55°C	Yes	****	<0.000000000000001	No	ns	>0.999999999999
L_{10nm}-55°C vs. L_{50nm}-55°C	Yes	****	<0.000000000000001	No	ns	0.999999982
L_{10nm}-55°C vs. L_{70nm}-55°C	Yes	****	<0.000000000000001	No	ns	0.99937119
L_{10nm}-55°C vs. L_{90nm}-55°C	Yes	****	<0.000000000000001	No	ns	0.539003525
L_{10nm}-55°C vs. L_{110nm}-55°C	Yes	****	<0.000000000000001	Yes	*	0.029530476
L_{10nm}-55°C vs. L_{110nm}(Δ32)-55°C	Yes	****	<0.000000000000001	No	ns	0.983240496
L_{30nm}-40°C vs. L_{50nm}-40°C	Yes	****	<0.000000000000001	No	ns	>0.999999999999
L_{30nm}-40°C vs. L_{70nm}-40°C	Yes	****	4.40394E-06	No	ns	>0.999999999999
L_{30nm}-40°C vs. L_{90nm}-40°C	Yes	****	1.5316E-11	No	ns	>0.999999999999
L_{30nm}-40°C vs. L_{110nm}-40°C	No	ns	0.752058186	No	ns	1
L_{30nm}-40°C vs. L_{110nm}(Δ32)-40°C	Yes	****	<0.000000000000001	No	ns	>0.999999999999
L_{30nm}-55°C vs. L_{50nm}-55°C	Yes	****	<0.000000000000001	No	ns	1
L_{30nm}-55°C vs. L_{70nm}-55°C	Yes	****	<0.000000000000001	No	ns	0.999915334
L_{30nm}-55°C vs. L_{90nm}-55°C	Yes	****	<0.000000000000001	No	ns	0.652751016
L_{30nm}-55°C vs. L_{110nm}-55°C	Yes	****	<0.000000000000001	Yes	*	0.046820994
L_{30nm}-55°C vs. L_{110nm}(Δ32)-55°C	Yes	****	<0.000000000000001	No	ns	0.99463928

L_{50nm}-40°C vs. L_{70nm}-40°C	Yes	***	0.000298267	No	ns	>0.999999999999
L_{50nm}-40°C vs. L_{90nm}-40°C	No	ns	0.337297518	No	ns	>0.999999999999
L_{50nm}-40°C vs. L_{110nm}-40°C	Yes	****	<0.000000000000001	No	ns	0.999999987
L_{50nm}-40°C vs. L_{110nm}(Δ32)-40°C	Yes	****	<0.000000000000001	No	ns	>0.999999999999
L_{50nm}-55°C vs. L_{70nm}-55°C	Yes	****	<0.000000000000001	No	ns	0.999998522
L_{50nm}-55°C vs. L_{90nm}-55°C	Yes	****	<0.000000000000001	No	ns	0.801620993
L_{50nm}-55°C vs. L_{110nm}-55°C	Yes	****	<0.000000000000001	No	ns	0.087276756
L_{50nm}-55°C vs. L_{110nm}(Δ32)-55°C	Yes	****	<0.000000000000001	No	ns	0.99939538
L_{70nm}-40°C vs. L_{90nm}-40°C	No	ns	0.998819081	No	ns	>0.999999999999
L_{70nm}-40°C vs. L_{110nm}-40°C	No	ns	0.067160378	No	ns	0.999999999
L_{70nm}-40°C vs. L_{110nm}(Δ32)-40°C	Yes	****	<0.000000000000001	No	ns	>0.999999999999
L_{70nm}-55°C vs. L_{90nm}-55°C	Yes	****	<0.000000000000001	No	ns	0.983141406
L_{70nm}-55°C vs. L_{110nm}-55°C	Yes	****	<0.000000000000001	No	ns	0.304753716
L_{70nm}-55°C vs. L_{110nm}(Δ32)-55°C	Yes	****	<0.000000000000001	No	ns	0.999999984
L_{90nm}-40°C vs. L_{110nm}-40°C	Yes	****	7.48871E-06	No	ns	1
L_{90nm}-40°C vs. L_{110nm}(Δ32)-40°C	Yes	****	<0.000000000000001	No	ns	>0.999999999999
L_{90nm}-55°C vs. L_{110nm}-55°C	Yes	****	<0.000000000000001	No	ns	1
L_{90nm}-55°C vs. L_{110nm}(Δ32)-55°C	Yes	****	<0.000000000000001	No	ns	0.999364715
L_{110nm}-40°C vs. L_{110nm}(Δ32)-40°C	Yes	****	<0.000000000000001	No	ns	0.99999998
L_{110nm}-55°C vs. L_{110nm}(Δ32)-55°C	Yes	****	<0.000000000000001	No	ns	0.561423678

Reference

1. Ye, X.; Zheng, C.; Chen, J.; Gao, Y.; Murray, C. B., Using binary surfactant mixtures to simultaneously improve the dimensional tunability and monodispersity in the seeded growth of gold nanorods. *Nano Lett.* **2013,** *13* (2), 765-71.
2. Orendorff, C. J.; Murphy, C. J., Quantitation of Metal Content in the Silver-Assisted Growth of Gold Nanorods. *The Journal of Physical Chemistry B* **2006,** *110* (9), 3990-3994.
3. Bazrafshan, A.; Meyer, T. A.; Su, H.; Brockman, J. M.; Blanchard, A. T.; Piranej, S.; Duan, Y.; Ke, Y.; Salaita, K., Tunable DNA Origami Motors Translocate Ballistically Over mum Distances at nm/s Speeds. *Angew Chem Int Ed Engl* **2020,** *59* (24), 9514-9521.
4. Ke, Y.; Meyer, T.; Shih, W. M.; Bellot, G., Regulation at a distance of biomolecular interactions using a DNA origami nanoactuator. *Nat. Commun.* **2016,** *7*, 10935.
5. Petrosyan, R., Improved approximations for some polymer extension models. *Rheol. Acta* **2017,** *56* (1), 21-26.
6. Zhang, Y.; Qiu, Y.; Blanchard, A. T.; Chang, Y.; Brockman, J. M.; Ma, V. P.; Lam, W. A.; Salaita, K., Platelet integrins exhibit anisotropic mechanosensing and harness piconewton forces to mediate platelet aggregation. *Proc. Natl. Acad. Sci. U.S.A* **2018,** *115* (2), 325-330.
7. Liedl, T.; Högberg, B.; Tytell, J.; Ingber, D. E.; Shih, W. M., Self-assembly of three-dimensional prestressed tensegrity structures from DNA. *Nat. Nanotechnol.* **2010,** *5*, 520.
8. Castro, C. E.; Su, H.-J.; Marras, A. E.; Zhou, L.; Johnson, J., Mechanical design of DNA nanostructures. *Nanoscale* **2015,** *7* (14), 5913-5921.
9. Woodside, M. T.; Behnke-Parks, W. M.; Larizadeh, K.; Travers, K.; Herschlag, D.; Block, S. M., Nanomechanical measurements of the sequence-dependent folding landscapes of single nucleic acid hairpins. *Proc. Natl. Acad. Sci. U.S.A* **2006,** *103* (16), 6190-5.
10. Bell, G. I., Models for the specific adhesion of cells to cells. *Science* **1978,** *200* (4342), 618-27.
11. Ouldridge, T. E.; Louis, A. A.; Doye, J. P. K., Structural, mechanical, and thermodynamic properties of a coarse-grained DNA model. *The Journal of chemical physics* **2011,** *134* (8), 085101.
12. Šulc, P.; Romano, F.; Ouldridge, T. E.; Rovigatti, L.; Doye, J. P. K.; Louis, A. A., Sequence-dependent thermodynamics of a coarse-grained DNA model. *The Journal of chemical physics* **2012,** *137* (13), 135101.
13. Snodin, B. E. K.; Randisi, F.; Mosayebi, M.; Šulc, P.; Schreck, J. S.; Romano, F.; Ouldridge, T. E.; Tsukanov, R.; Nir, E.; Louis, A. A.; Doye, J. P. K., Introducing improved structural properties and salt dependence into a coarse-grained model of DNA. *The Journal of chemical physics* **2015,** *142* (23), 234901.
14. Snodin, B. E. K.; Schreck, J. S.; Romano, F.; Louis, A. A.; Doye, J. P. K., Coarse-grained modelling of the structural properties of DNA origami. *Nucleic acids research* **2019,** *47* (3), 1585-1597.
15. Bai, X.-c.; Martin, T. G.; Scheres, S. H. W.; Dietz, H., Cryo-EM structure of a 3D DNA-origami object. *Proc. Natl. Acad. Sci. U.S.A* **2012,** *109* (49), 20012-20017.
16. Chhabra, H.; Mishra, G.; Cao, Y.; Prešern, D.; Skoruppa, E.; Tortora, M. M. C.; Doye, J. P. K., Computing the Elastic Mechanical Properties of Rodlike DNA Nanostructures. *Journal of chemical theory and computation* **2020,** *16* (12), 7748-7763.

17. Engel, M. C.; Smith, D. M.; Jobst, M. A.; Sajfutdinow, M.; Liedl, T.; Romano, F.; Rovigatti, L.; Louis, A. A.; Doye, J. P. K., Force-Induced Unravelling of DNA Origami. *ACS Nano* **2018,** *12* (7), 6734-6747.
18. Romano, F.; Chakraborty, D.; Doye, J. P. K.; Ouldridge, T. E.; Louis, A. A., Coarse-grained simulations of DNA overstretching. *The Journal of chemical physics* **2013,** *138* (8), 085101.
19. Mosayebi, M.; Romano, F.; Ouldridge, T. E.; Louis, A. A.; Doye, J. P. K., The Role of Loop Stacking in the Dynamics of DNA Hairpin Formation. *The Journal of Physical Chemistry B* **2014,** *118* (49), 14326-14335.
20. Engel, M. C.; Romano, F.; Louis, A. A.; Doye, J. P. K., Measuring Internal Forces in Single-Stranded DNA: Application to a DNA Force Clamp. *Journal of chemical theory and computation* **2020,** *16* (12), 7764-7775.
21. Nickels, P. C.; Wunsch, B.; Holzmeister, P.; Bae, W.; Kneer, L. M.; Grohmann, D.; Tinnefeld, P.; Liedl, T., Molecular force spectroscopy with a DNA origami-based nanoscopic force clamp. *Science* **2016,** *354* (6310), 305-307.
22. Rovigatti, L.; Šulc, P.; Reguly, I. Z.; Romano, F., A comparison between parallelization approaches in molecular dynamics simulations on GPUs. *Journal of Computational Chemistry* **2015,** *36* (1), 1-8.
23. Russo, J.; Tartaglia, P.; Sciortino, F., Reversible gels of patchy particles: Role of the valence. *The Journal of chemical physics* **2009,** *131* (1), 014504.
24. Kube, M.; Kohler, F.; Feigl, E.; Nagel-Yüksel, B.; Willner, E. M.; Funke, J. J.; Gerling, T.; Stömmer, P.; Honemann, M. N.; Martin, T. G.; Scheres, S. H. W.; Dietz, H., Revealing the structures of megadalton-scale DNA complexes with nucleotide resolution. *Nature Communications* **2020,** *11* (1), 6229.
25. Cooper, M.; Ebner, A.; Briggs, M.; Burrows, M.; Gardner, N.; Richardson, R.; West, R., Cy3B: improving the performance of cyanine dyes. *J Fluoresc* **2004,** *14* (2), 145-50.
26. Sato Matsuo, E.; Tanaka, T., Kinetics of discontinuous volume–phase transition of gels. *The Journal of chemical physics* **1988,** *89* (3), 1695-1703.
27. Wang, J.; Gan, D.; Lyon, L. A.; El-Sayed, M. A., Temperature-jump investigations of the kinetics of hydrogel nanoparticle volume phase transitions. *J. Am. Chem. Soc* **2001,** *123* (45), 11284-9.
28. Reese, C. E.; Mikhonin, A. V.; Kamenjicki, M.; Tikhonov, A.; Asher, S. A., Nanogel nanosecond photonic crystal optical switching. *J. Am. Chem. Soc* **2004,** *126* (5), 1493-6.
29. Ahmed, Z.; Gooding, E. A.; Pimenov, K. V.; Wang, L.; Asher, S. A., UV resonance Raman determination of molecular mechanism of poly(N-isopropylacrylamide) volume phase transition. *J Phys Chem B* **2009,** *113* (13), 4248-56.
30. Wu, T. Y.; Zrimsek, A. B.; Bykov, S. V.; Jakubek, R. S.; Asher, S. A., Hydrophobic Collapse Initiates the Poly(N-isopropylacrylamide) Volume Phase Transition Reaction Coordinate. *J Phys Chem B* **2018,** *122* (11), 3008-3014.
31. Wahrmund, J.; Kim, J.-W.; Chu, L.-Y.; Wang, C.; Li, Y.; Fernandez-Nieves, A.; Weitz, D. A.; Krokhin, A.; Hu, Z., Swelling Kinetics of a Microgel Shell. *Macromolecules* **2009,** *42* (23), 9357-9365.
32. Suarez, I. J.; Fernandez-Nieves, A.; Marquez, M., Swelling kinetics of poly(N-isopropylacrylamide) minigels. *J Phys Chem B* **2006,** *110* (51), 25729-33.

33. Zhao, J.; Su, H.; Vansuch, G. E.; Liu, Z.; Salaita, K.; Dyer, R. B., Localized Nanoscale Heating Leads to Ultrafast Hydrogel Volume-Phase Transition. *ACS Nano* **2019,** *13* (1), 515-525.